SAND Software and Analysis

Matteo Tenti, INFN - Bologna

SAND Review CSN1
12/07/2024 Frascati

Introduction

Meetings

- The Physics/Software WG (16 people) has regular weekly meetings: Wednesday at 15:00 CEST (08:00 CT)
- A shared google docs is used to take notes
- Meetings are recorded
- A list of action items is produced and checked during the meeting
- Two mailing lists:
  - DUNE-ND-SAND-PHYSICS@FNAL.GOV
  - DUNE-ND-SAND-SOFTWARE@FNAL.GOV

Repositories

- github.com/DUNE/dunendggd:
  geometry repository

- github.com/DUNE/sandreco
  detector simulation, reconstruction and analysis tools

- github.com/DUNE/ND_Production
  ND «official production» for simulation

- github.com/DUNE/ND_CAFMaker
  CAF maker: event summary data

Coding and Development Workflow

- Language: C++11
- Code Format:
  - Based on [Google C++ Style Guide]
  - Proposal: *clang-format -style="{BasedOnStyle: Google, BreakBeforeBraces: Linux, DerivePointerAlignment: false}"*
- Project layout: [pitchfork]
- Development Workflow:
  1. Create Issue
  2. Open Branch
  3. Develop
  4. Test / Review
  5. Merge Request
  6. Release

Exploits:
Agile/DevOps,
Merging by Pull Request
Peer Code Review,
Automated Tests,

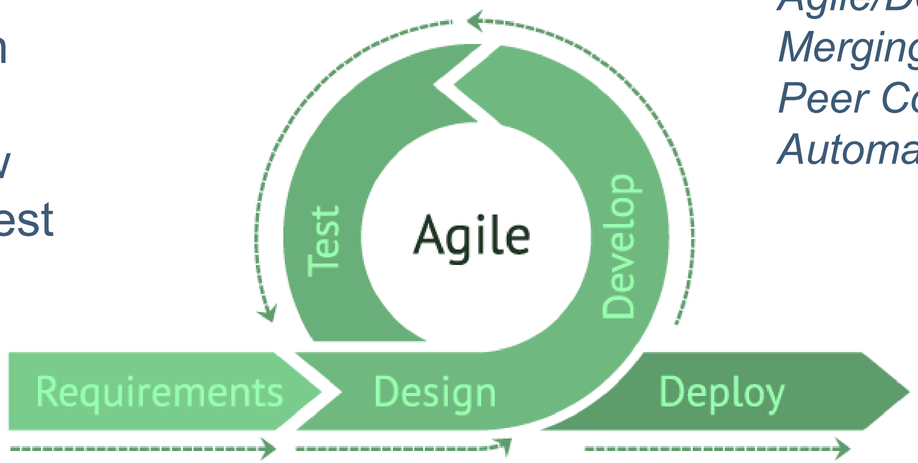

SAND Geometry

SAND Geometry

- SANDGeoManager
- Easy tool to build geometry w/ gegede

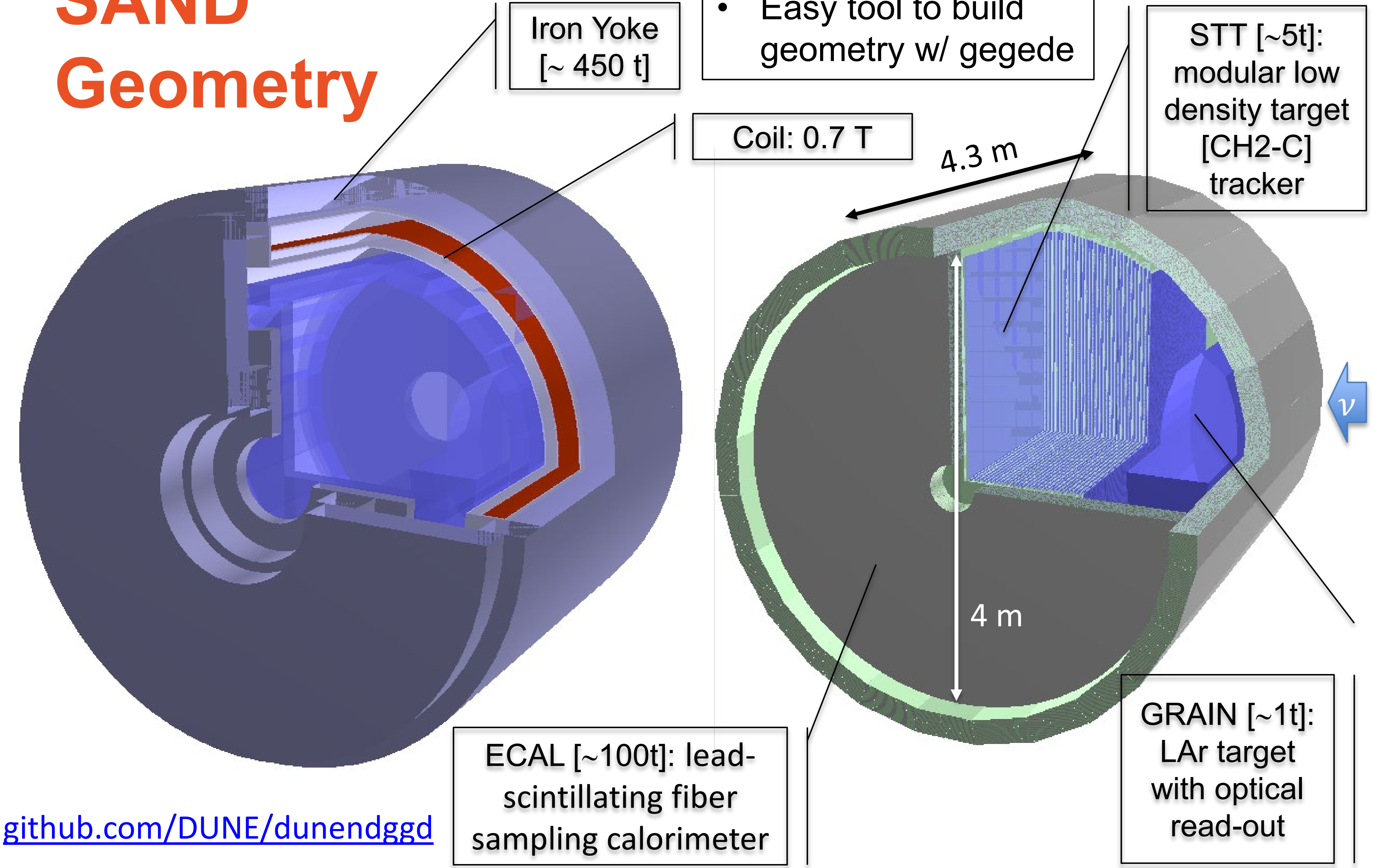

github.com/DUNE/dunendggd

Tracker Modules

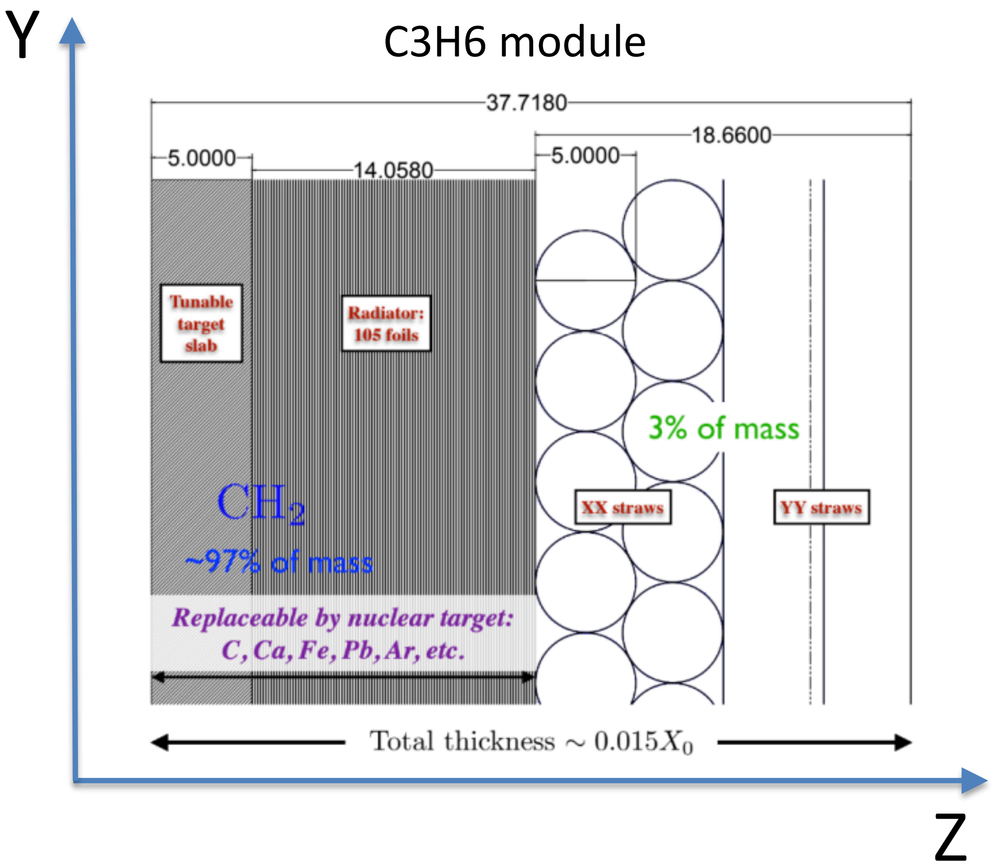

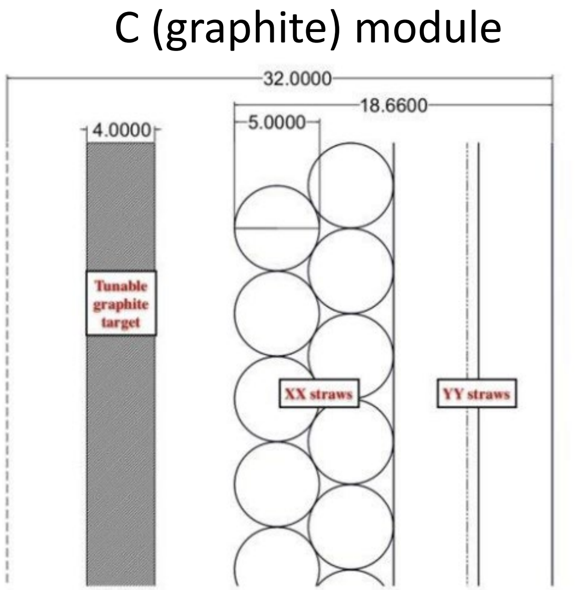

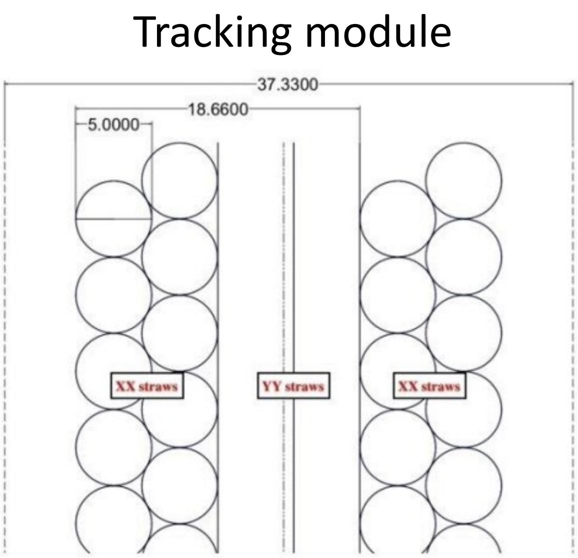

Different options for tracker

Straw tubes

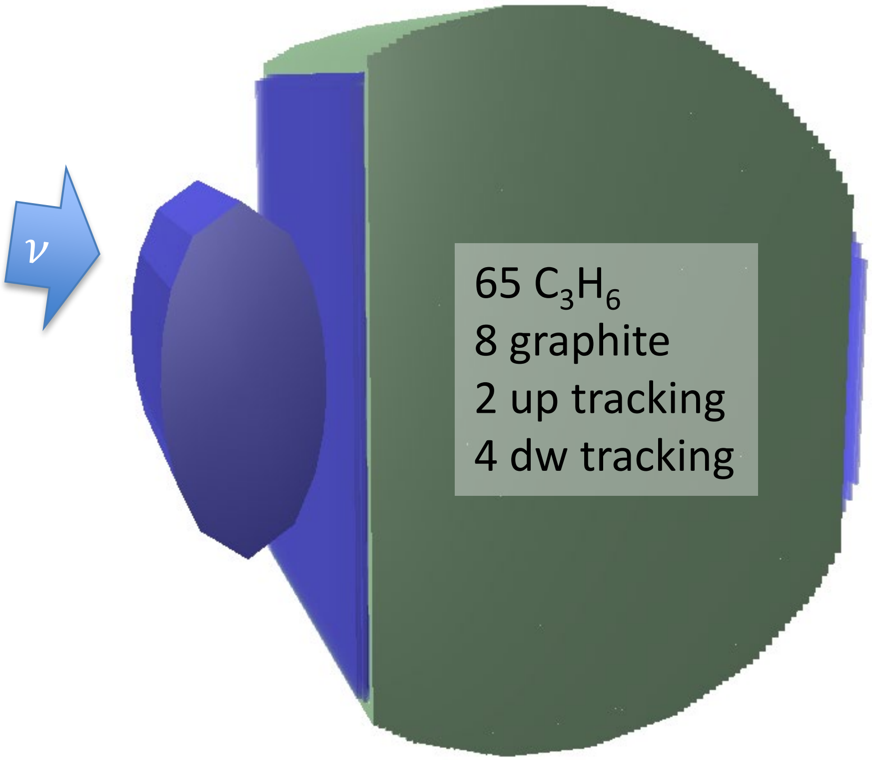

Drift chambers

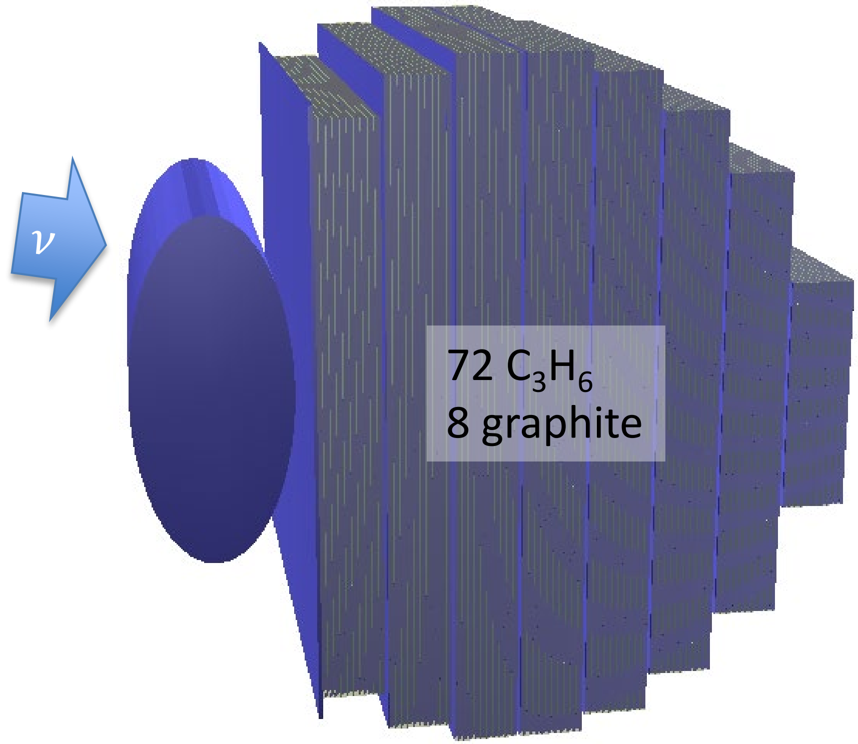

Geometries with several tracker configuration:
clearance, straw radius, GRAIN size, TR removal

ECAL Geometry

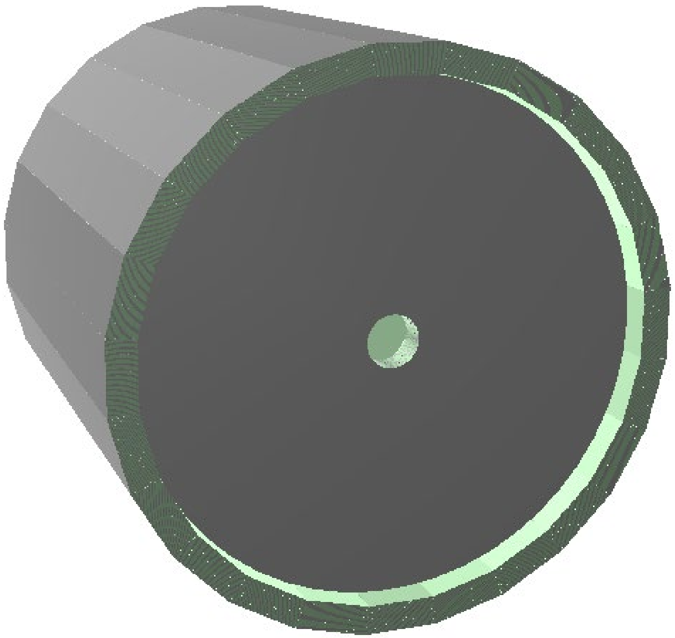

Improved endcap geometry
[P. Gauzzi]

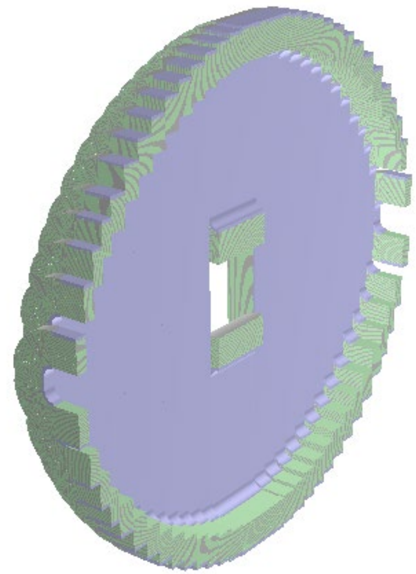

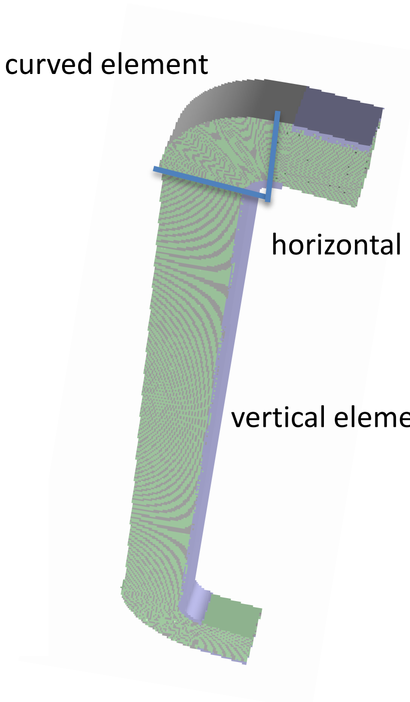

Barrel: 24 modules

2 x Endcaps: 32 modules

Module:

- 209 0.4-mm lead slabs +
- 209 0.7-mm scint. slabs

A team (**P. Gauzzi, A. Ruggeri, D. Casazza, M. Tenti**) is working to finalize the digitization for the new endcap geometry

SAND Simulation & Reconstruction

Reconstruction Chain: Full

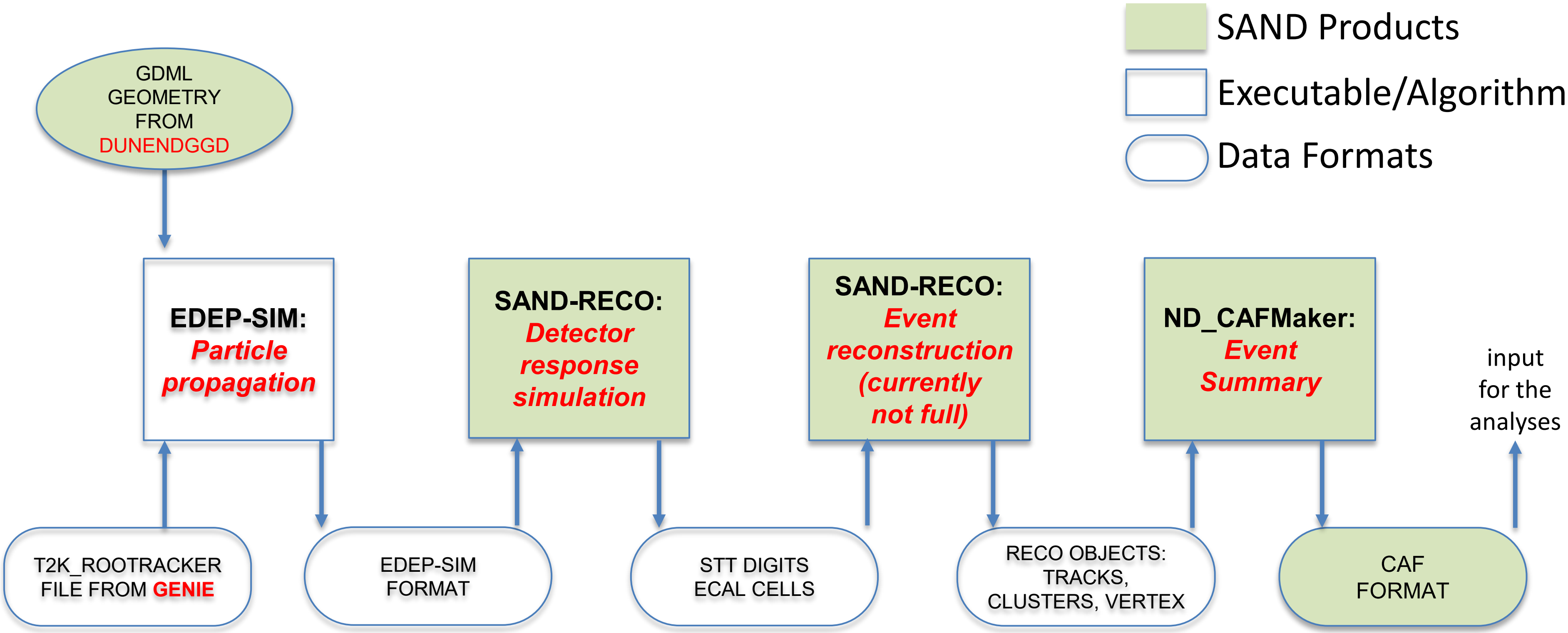

Ref. GENIE Manual

Ref. EDEP-SIM output

Ref. sand-reco wiki

Ref. sand-reco wiki

Ref. ND_CAFMaker repo

Detector Simulation

- ECAL [sand-reco]:
  - Light yield, scintillation decay time, attenuation, photon propagation, segmentation, PMT response and front-end [ADC & TDC].

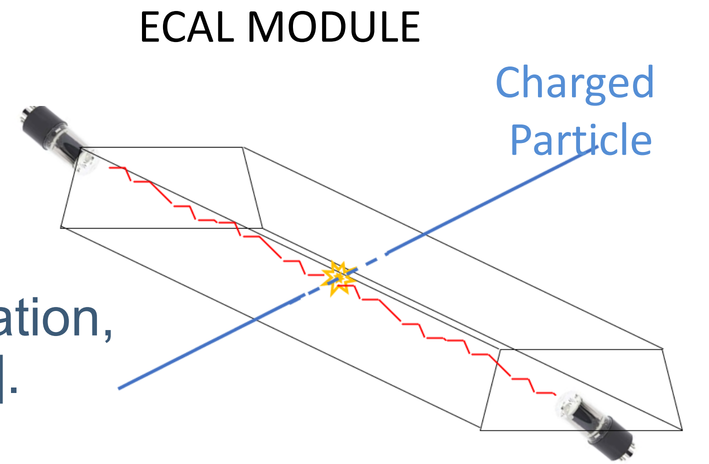

- STRAW/DRIFT[sand-reco]:
  - drift towards wire, electric signal propagation and front-end [ADC & TDC]

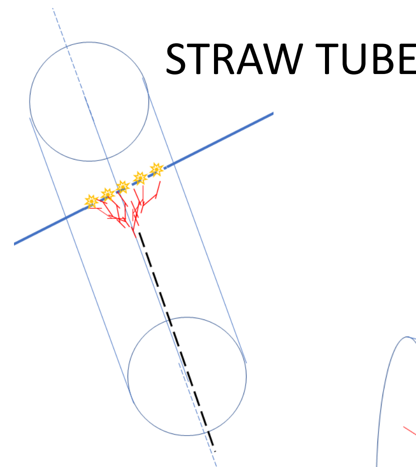

- GRAIN:
  - LAr : Rayleigh scattering, absorption
    SiPM : PDE, cross-talk, after-pulse
    front-end : waveform with electronic noise

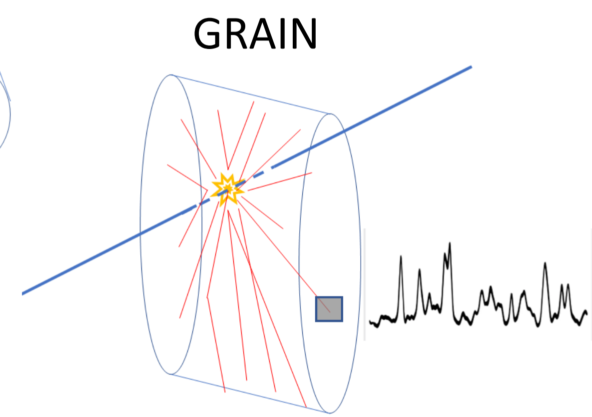

Reconstruction

[D. Casazza, R. D'Amico, P. Gauzzi]

- ECAL:
  - CELL: Energy, position and time of energy deposits in ECAL are reconstructed using signals of PMTs on both ends.
  - PATTERN RECOGNITION: CELLS are grouped in CLUSTERS using MC truth.
  - FIT: Energy, position, time and direction of the track/shower are then reconstructed using energy deposit topologie

t_{cell} for 10 GeV muons

$$\sigma_t = \frac{54\ ps}{\sqrt{E(GeV)}}$$

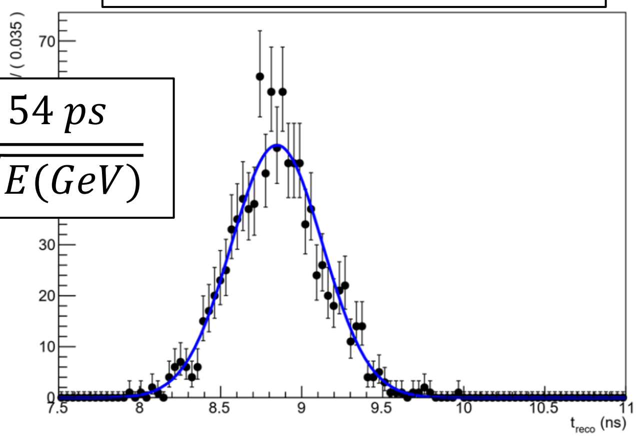

adc_{cell} for 1 GeV e^-

$$\sigma_E = \frac{5\ \%}{\sqrt{E(GeV)}}$$

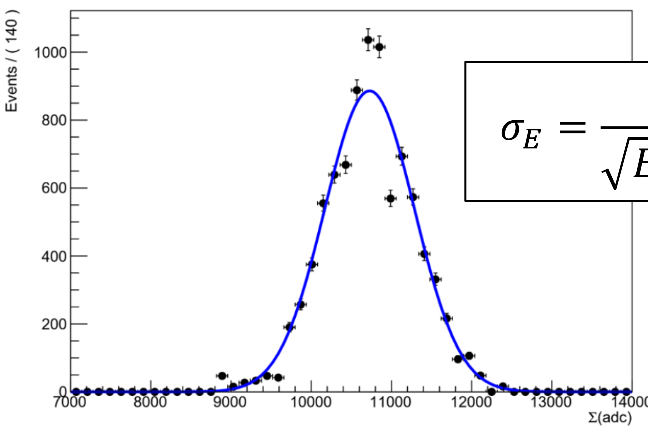

Reconstruction

- STT
  - PATTERN RECOGNITION: TUBES are grouped in TRACKS using MC truth.
  - FIT: hits from vertical and horizontal tubes are fitted separately to obtain position direction and momentum of the TRACK

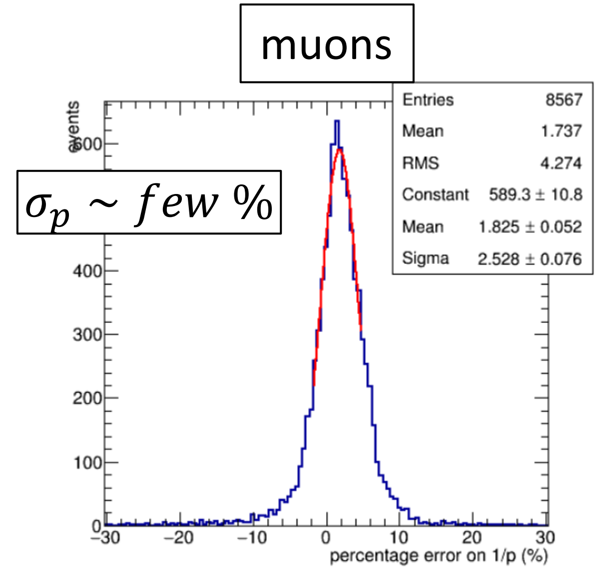

- GRAIN

3D reconstruction with **Multiple View**

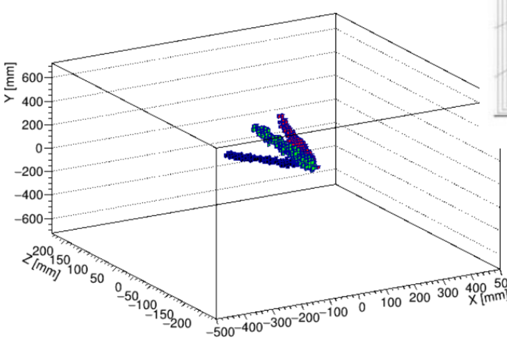

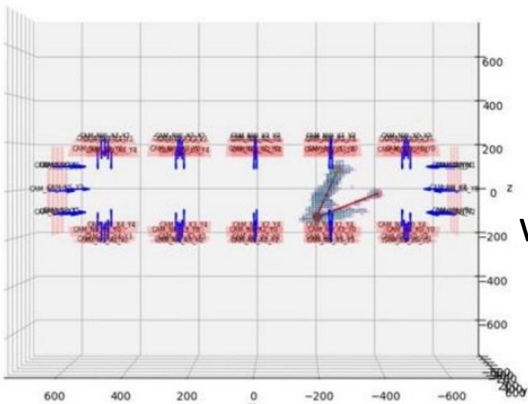

3D reconstruction with **Back Propagation**

2D reconstruction with **Hough Transform**

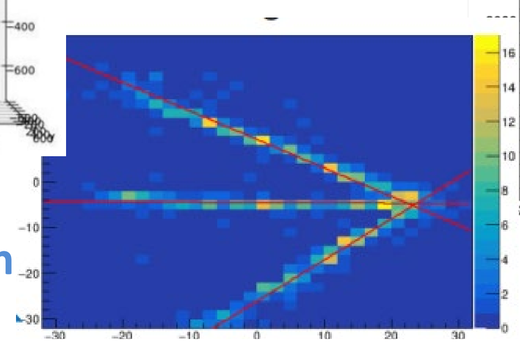

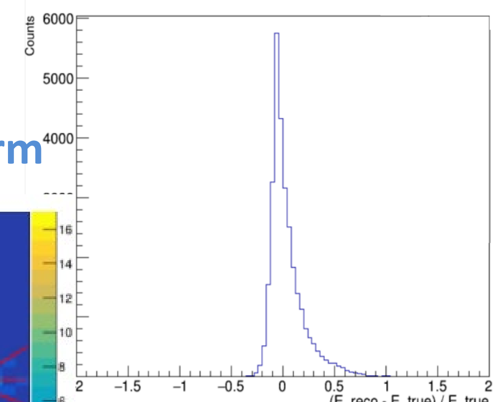

Calorimetry

Reconstruction Chain: Fast

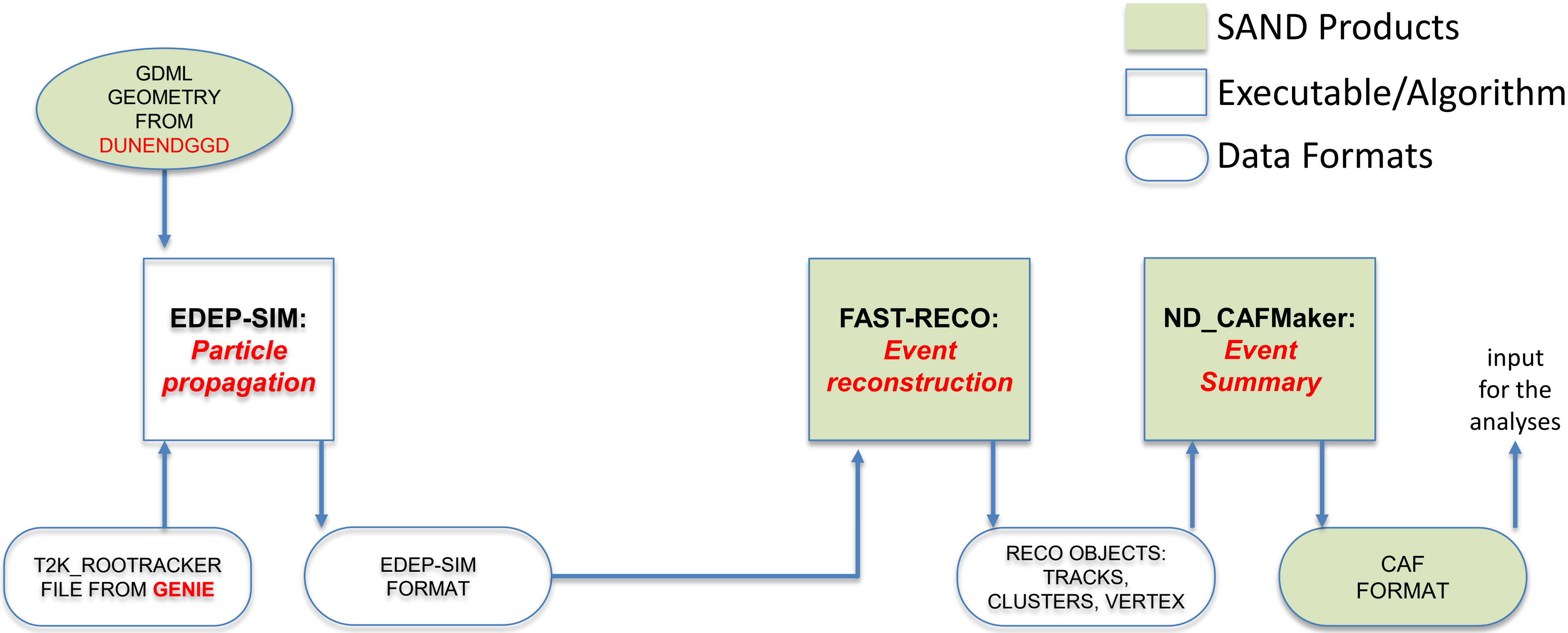

Ref. [GENIE Manual]

Ref. [EDEP-SIM output]

Ref. [sand-reco wiki]

Ref. [ND_CAFMaker repo]

Fast Reconstruction

- A (simplified) fast reconstruction has been developped to quickly obtain reliable results
- Basic ingredients:
  - Detection thresholds:
    - 250 eV for straw
    - 100 keV of deposited energy in fibers (equivalent to ~ 1 MeV in cell)
  - Tracks:
    - Reconstruction threshold N(digitis) > 4
    - Pattern recognition and PID from MC truth
    - Reconstructed momentum using Gluckstern formula
  - Gammas' energy: $(5.6\%)/\sqrt{(E/GeV)}$ on visible energy in ECAL
  - Neutrons' energy: TOF

GRAIN: Masks

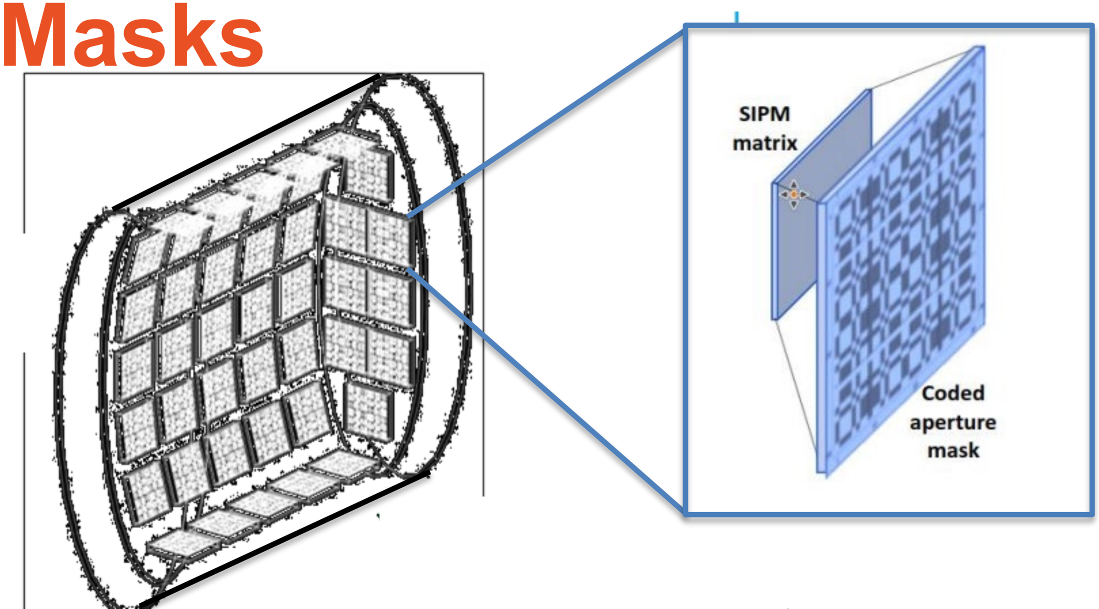

SIPM matrix
Coded aperture mask

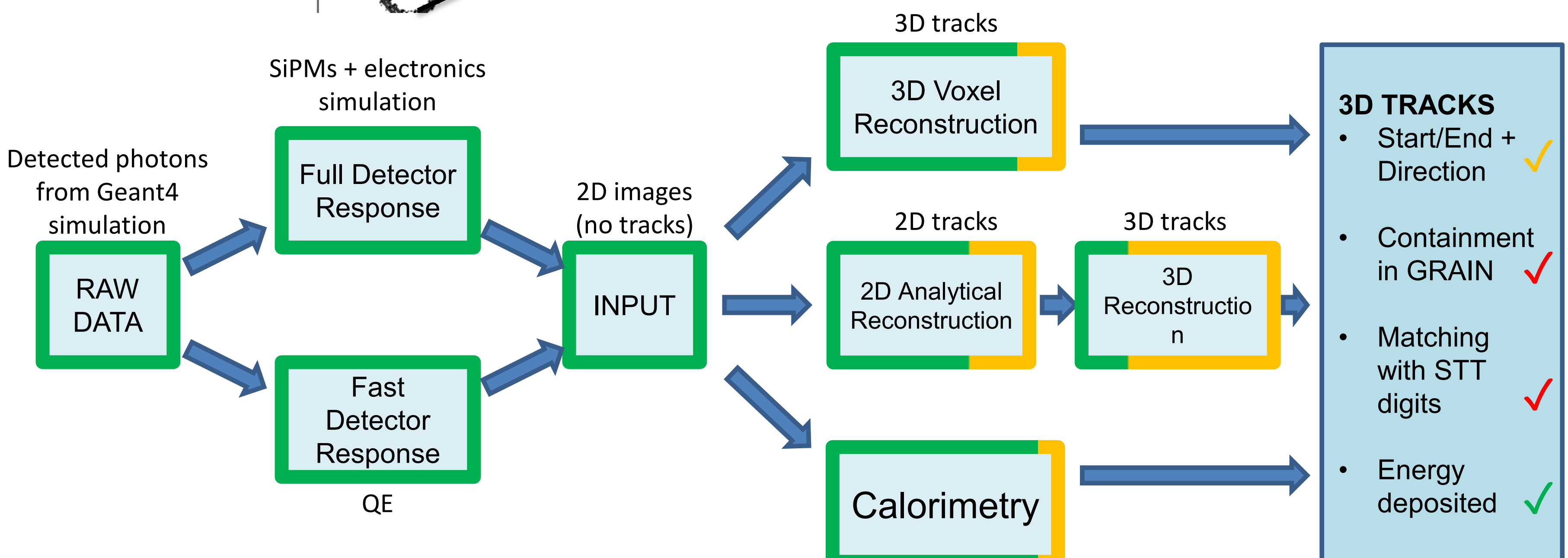

Detected photons from Geant4 simulation
RAW DATA
SiPMs + electronics simulation
Full Detector Response
Fast Detector Response
QE
2D images (no tracks)
INPUT
3D tracks
3D Voxel Reconstruction
2D tracks
2D Analytical Reconstruction
3D tracks
3D Reconstructio n
Calorimetry
3D TRACKS
• Start/End + Direction ✓
• Containment in GRAIN ✓
• Matching with STT digits ✓
• Energy deposited ✓

GRAIN: Lenses

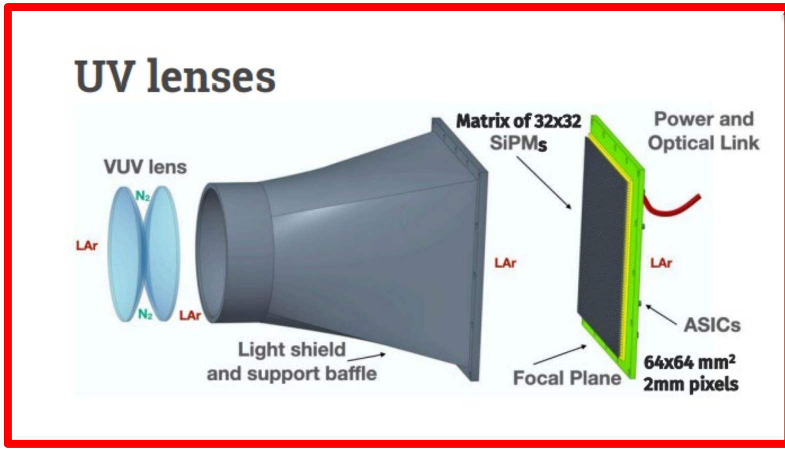

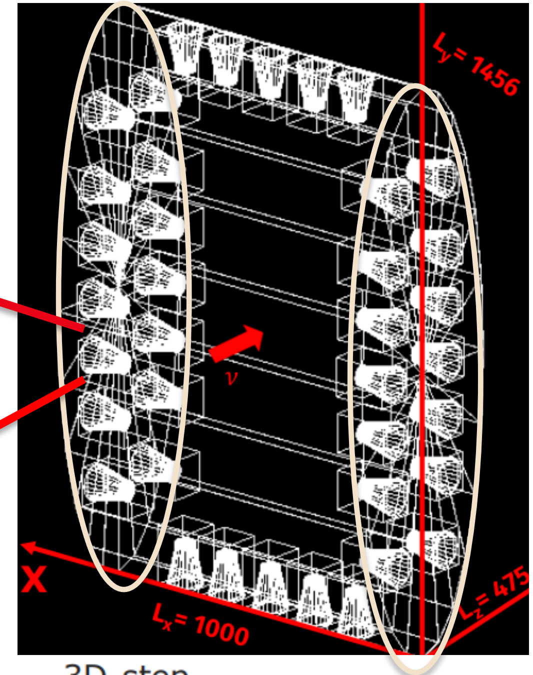

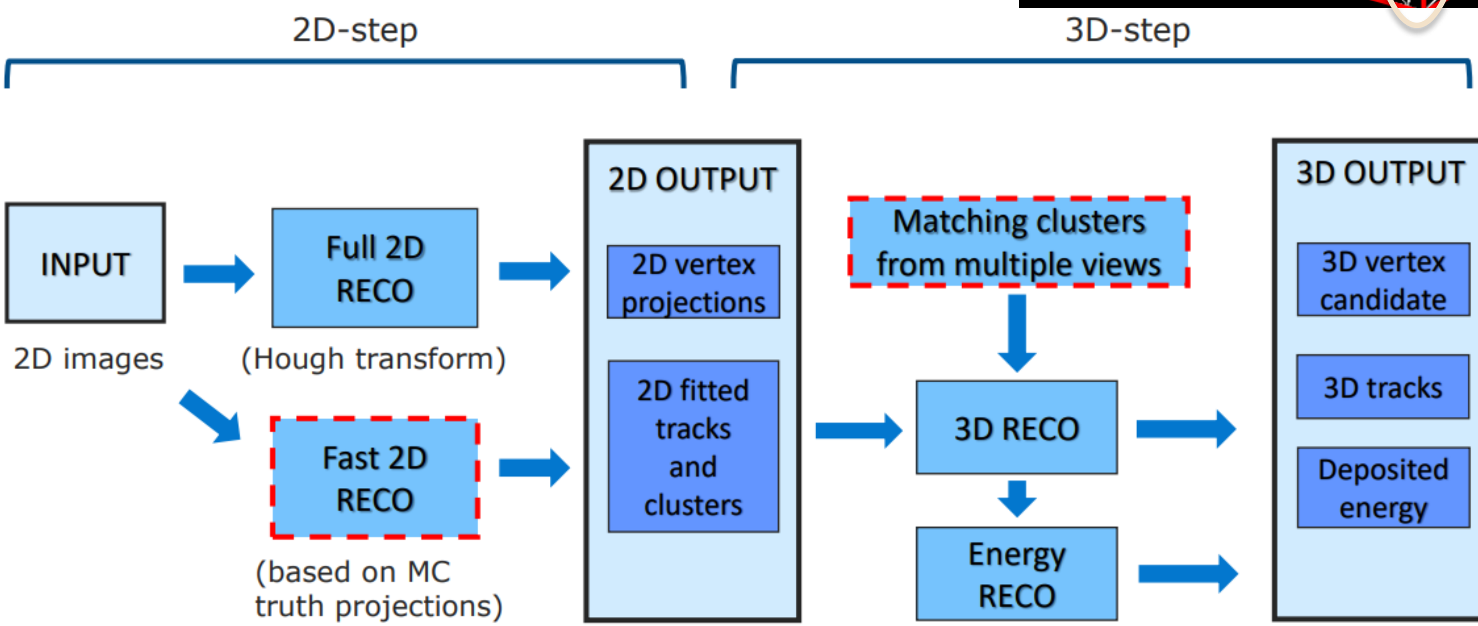

Event Viewers

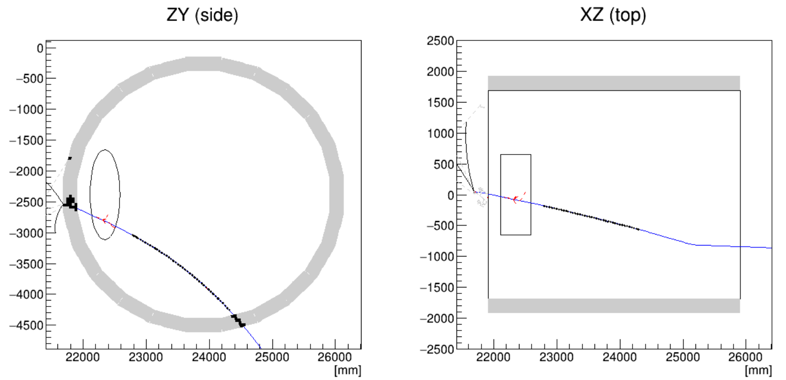

Simple single event display based on ROOT 2D basic graphics

[V. Pia]

Interactive display based **Qt** libraries

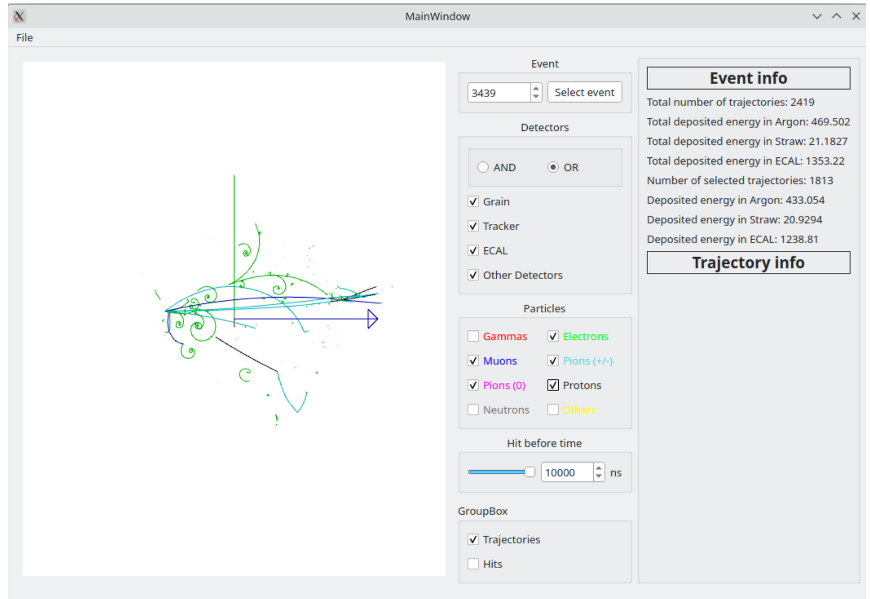

[A. Chukanov]

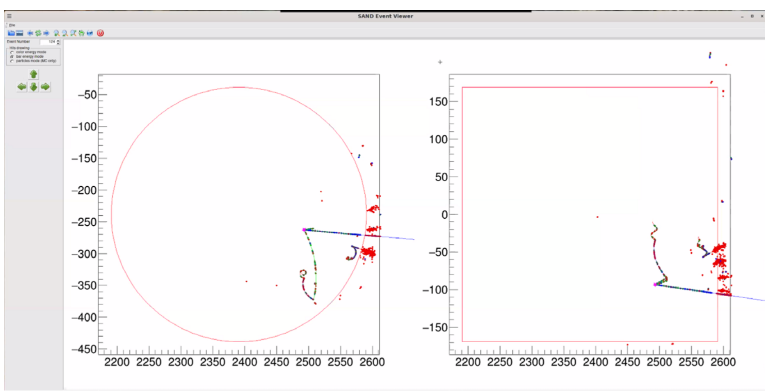

Interactive display based on **ROOT Graphical User Interface**

Integration in DUNE

Interfaces with DUNE

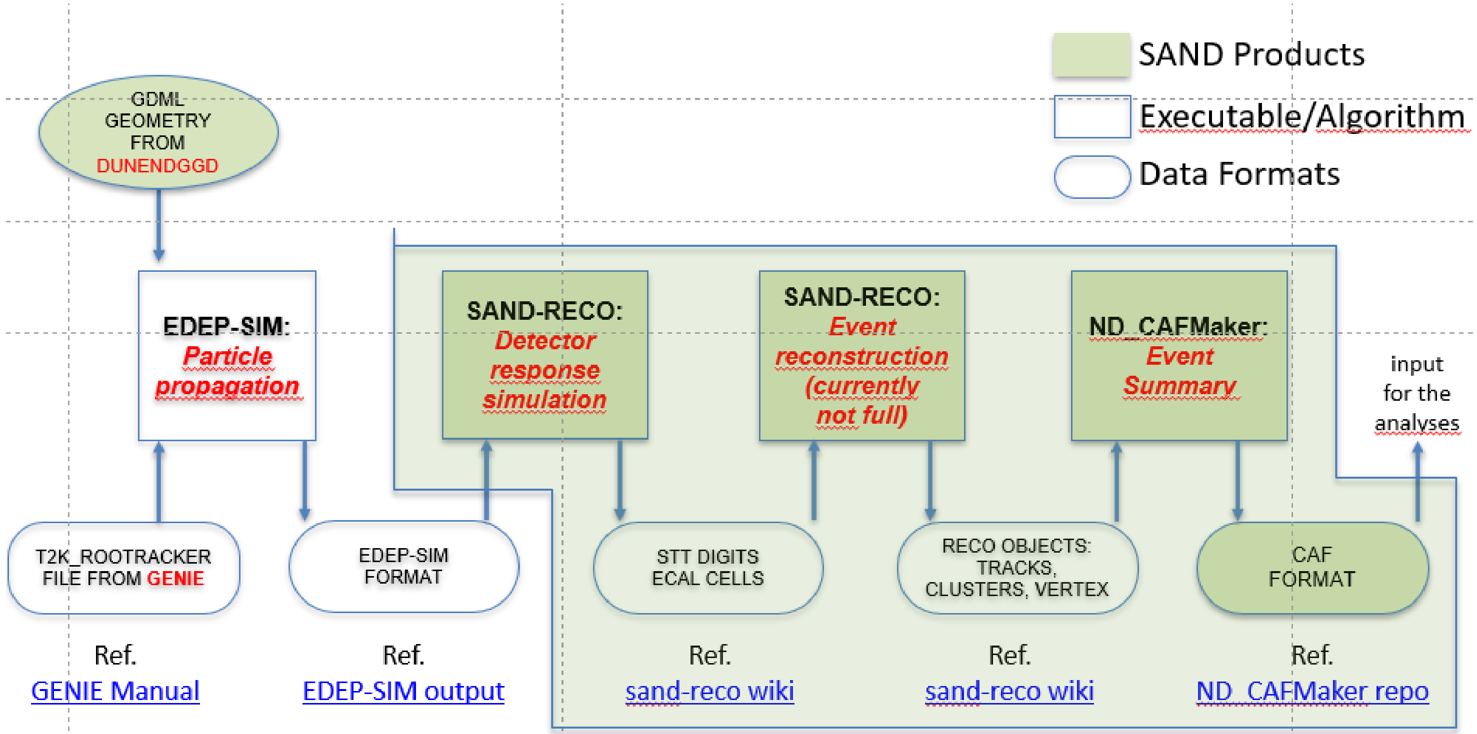

The green area is responsability of the SAND Physics/Software WG

- sandreco: continuous integration, testing, versioning and release
- Integration into ND simulation and reconstruction chain
- Development of an *event summary data*: CAF

CAF Updates Highlights

Proposed Design

```
/// Common Analysis Files
namespace caf
{

  /// \brief   The StandardRecord is the primary top-level object in the
  ///          Common Analysis File trees.
  class StandardRecord
  {
    public:
      /// Metadata about the detectors
      SRDetectorMetaBranch meta;

      /// Information about the beam configuration and beam pulse for this event
      SRBeamBranch beam;

      /// Truth information
      SRTruthBranch mc;

      /// Reconstructed info expected to be common to all (?) detectors
      SRCommonRecoBranch common;

      /// Reconstructed info unique to the FDs
      SRFDBranch fd;

      /// Reconstructed info u
      SRNDBranch nd;

  };
```

```
class SRNDBranch
{
  public:
    SRNDLAr   lar;
    SRGAr     gar;
    SRTMS     tms;
    SRSAND    sand;

    /// MINERvA detector pieces used in conjunction
    /// with 2x2 prototype in NuMI beam
    SRMINERvA minerva;

    std::size_t ntrkmatch = 0;
    std::vector<caf::SRNDTrackAssn> trkmatch;
};
```

- **Common Analysis Files** are the input for high-level analysis (used for TDR LBL analysis and by CAFAna, Mach3, etc…)
- Event Summary format is **StandardRecord** object
- It contains **SAND-related** objects and info
- Currently, we have a skeleton with minimal event info **[L. Di Noto]**
- We are involved in developing a complete CAF for SAND

[M. Tenti]

Integration in DUNE

- ND Sim/Reco group requests for an **integration** of the SAND simulation and reconstruction tools into the production chain
- A first integration of the SAND has been **completed**
- This includes ***Fast-Reco*** and ***sand-reco*** but not GRAIN reconstruction
- However, FNAL computing service has recently upgraded machines from SL7 to AL9
- In parallel, they decide to change the package manager from UPS (custom product) to Spack
- We are working to integrate *sandreco* in the new framework

Analysis

Particle Reconstruction

p_μ resolution

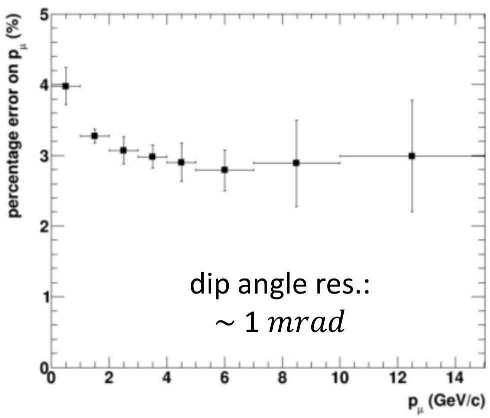

e^- mom. resolution

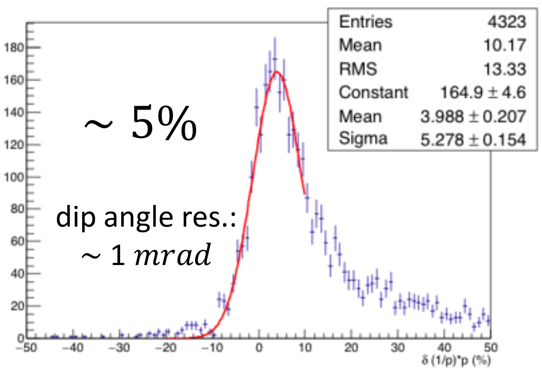

π^0 inv. Mass

$\sigma \sim 13\%$

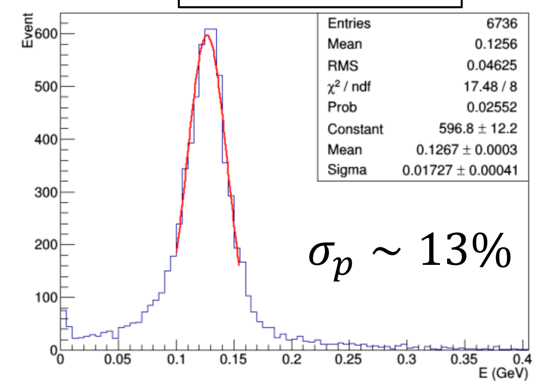

proton reco efficiency

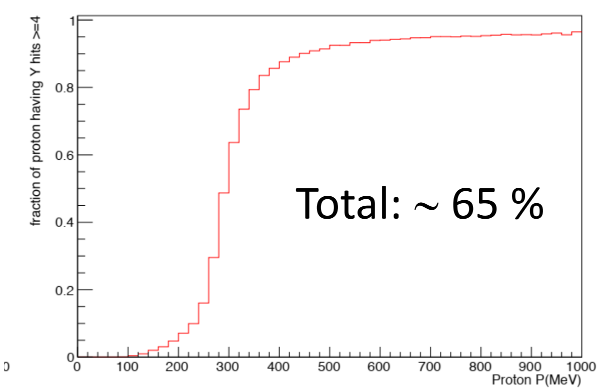

π^0 mom. reconstruction

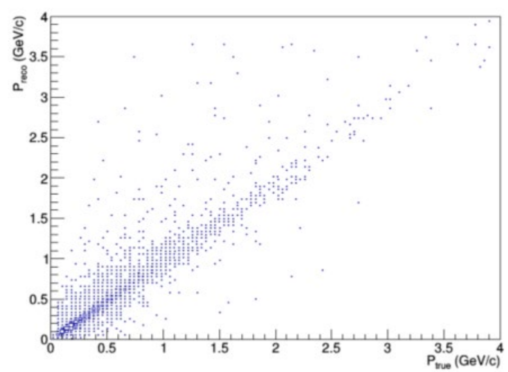

Neutron detection eff.

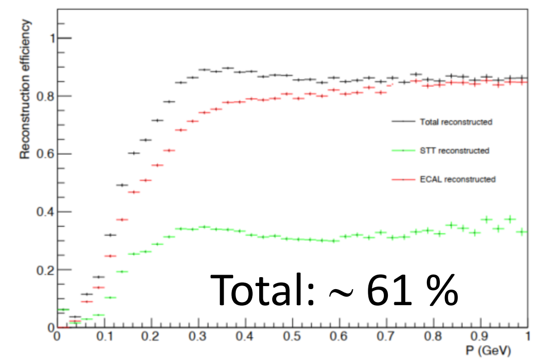

Particle Identification

***e/π* separation**
In addition to TR, **ECAL** could be used for e⁻ ID

***p/π* separation**
Combination of dE/dx, momentum and range

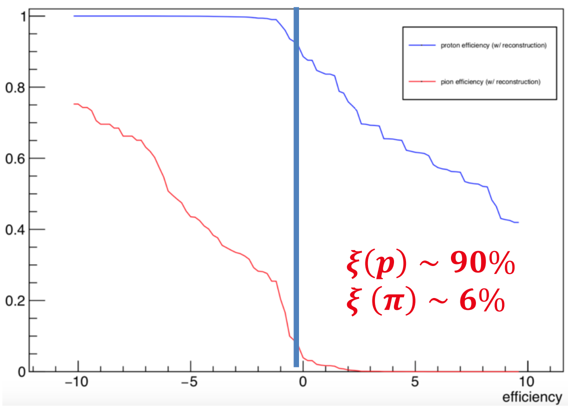

***μ/π* separation**
Use of topological variable of the energy deposit in ECAL

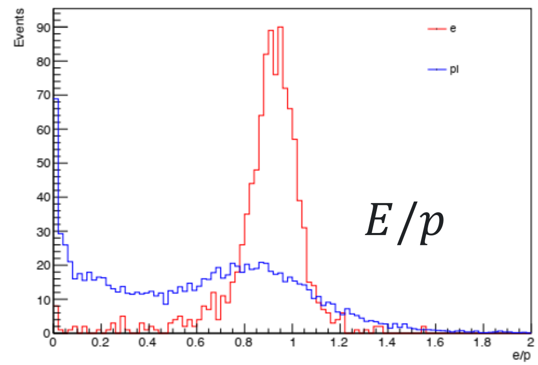

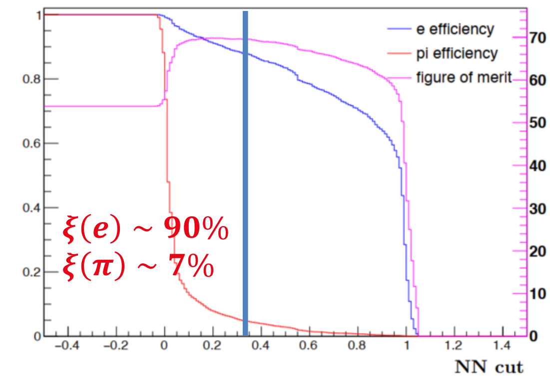

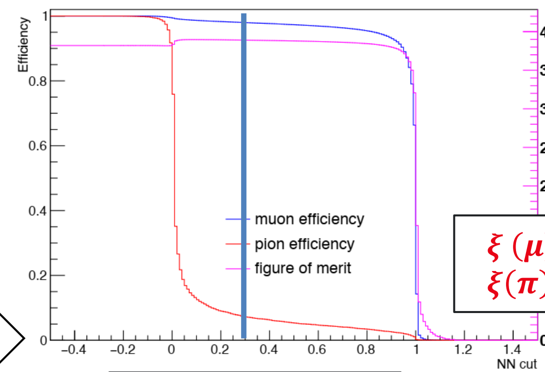

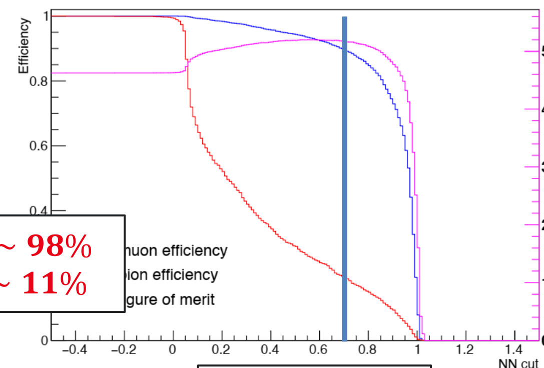

$\xi(\mu) \sim 98\%$
$\xi(\pi) \sim 11\%$

Stopping before ECAL Layer 4

For π exiting ECAL $\xi \sim 43\%$ Need for ext. μ catcher

Stopping in ECAL Layer 4

[docdb-13262]

Full Reconstruction Study

$$u = \frac{z - z_v}{(z - z_v)^2 + (y - y_v)^2}$$
$$v = -\frac{y - z_v}{(z - z_v)^2 + (y - y_v)^2}$$

- Iterative procedure
- First rough interaction vertex (z_v, y_v) determination using the spread profile of the STT hits

[A. Surdo & F. Alemanno]

first vtx estimation

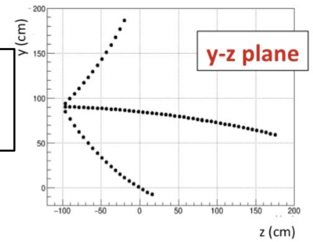

global transform method

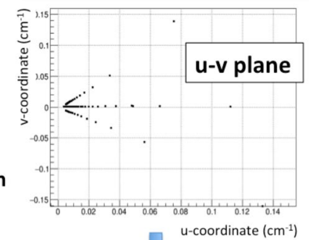

ϕ = atan(v/u)

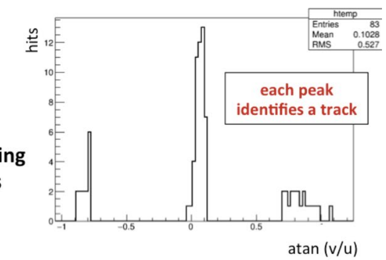

track finding and fits

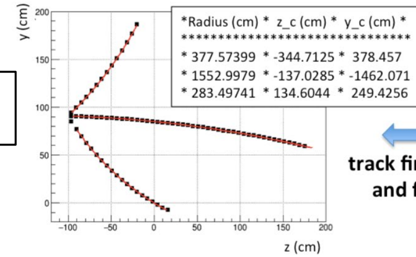

new vtx estimation

$\sigma_x \sim 210\ \mu m$

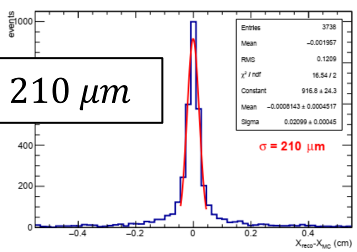

$\sigma_y \sim 370\ \mu m$

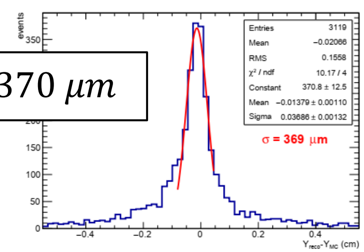

$\sigma_z \sim 690\ \mu m$

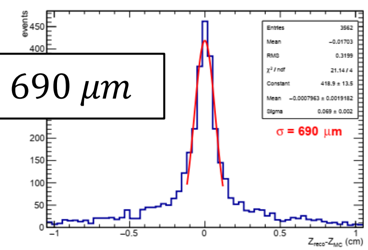

Resolution on vertex position

E_ν from reco tracks

$\sigma_E \sim 6\ \%$

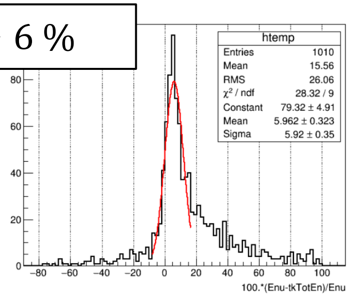

w/ off-track energy deposition in ECAL

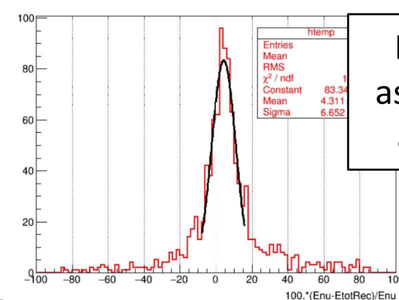

Reduced asymmetry and bias

docdb-13262

Events in an entire spill

PARTICLE level

(not time-gated)

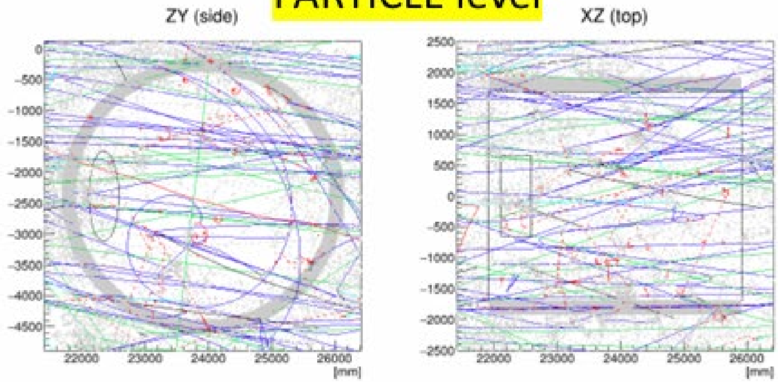

DIGITS level

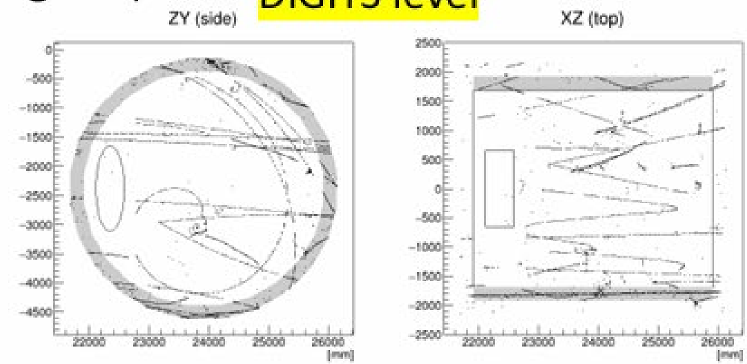

SAND + TMS + NDLAR (no rock-muon)

time-gated 100 ns

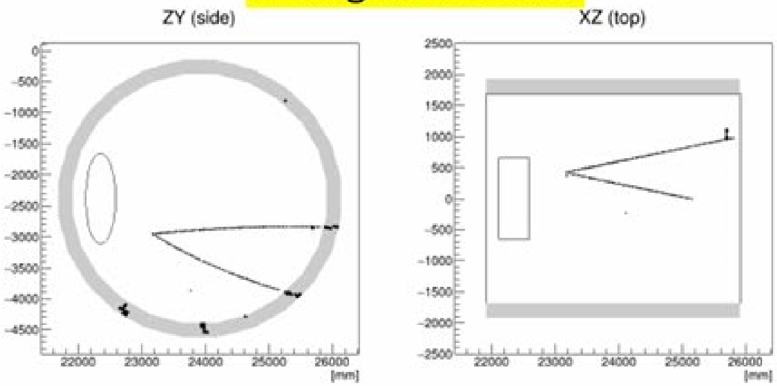

RECO level input

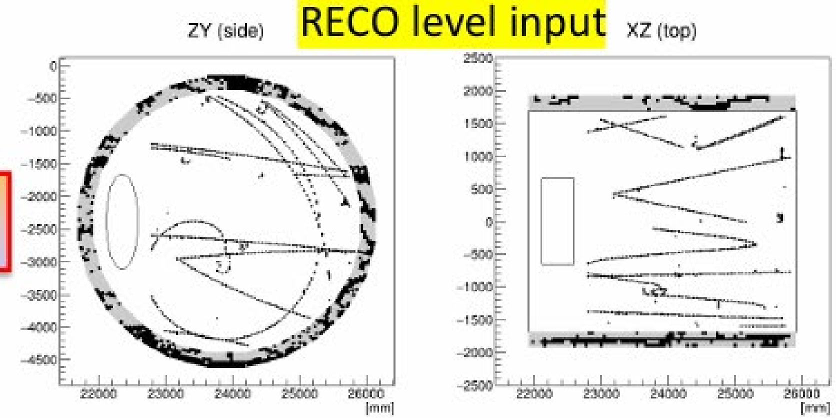

Event identified

Event Classification

- Primary lepton identification using ANN with kinematical variables

FHC ν_μ CC	99.1 %
RHC $\bar{\nu}_\mu$ CC	99.3 %
FHC ν_e CC	98.0 %
RHC $\bar{\nu}_e$ CC	98.6 %

- Additional ν_μ $(\bar{\nu}_\mu)$ selections based on:
  - μ catcher and μ/π separation w/ ECAL
  - Likelihood ratio based on kinematics (NC rejection)
- Additional ν_e $(\bar{\nu}_e)$ selections based on:
  - Invariant mass and e/π separation
  - Transition Radiation

Cuts	Efficiency	Purity $(\nu_\mu + \bar{\nu}_\mu + \nu_e + \bar{\nu}_e)$ CC + NC	Wrong sign contamination
FHC ν_μ CC selection:			
Kinematic tagging of μ^-	99.1 %	93.2 %	1.4 %
ECAL on tagged μ^-	98.4 %	97.5 %	0.5 %
RHC $\bar{\nu}_\mu$ CC selection:			
Kinematic tagging of μ^+	99.3 %	76.2 %	11.1 %
ECAL on tagged μ^+	98.8 %	90.0 %	6.1 %
Wrong sign veto on tagged μ^-	97.9 %	97.8 %	0.3 %
RHC ν_μ CC selection:			
Kinematic tagging of μ^-	98.7 %	66.4 %	22.7 %
ECAL on tagged μ^-	97.9 %	85.8 %	9.4 %
Wrong sign veto on tagged μ^+	95.4 %	97.3 %	0.3 %
FHC $\bar{\nu}_\mu$ CC selection:			
Kinematic tagging of μ^+	99.3 %	9.9 %	78.0 %
ECAL on tagged μ^+	98.2 %	34.2 %	55.1 %
Wrong sign veto on tagged μ^-	97.1 %	83.2 %	2.3 %
Kinematics	95.4 %	94.2 %	2.6 %

Cuts	Efficiency	Purity $(\nu_\mu + \bar{\nu}_\mu + \nu_e + \bar{\nu}_e)$ CC + NC
FHC ν_e CC selection:		
Kinematic tagging of e^-	98.0 %	1.3 %
Muon veto on tagged e^- and e^+	96.6 %	10.6 %
m_{+-} and ECAL on tagged e^-	91.8 %	27.3 %
TR + dE/dx on tagged e^-	82.6 %	99.4 %
RHC $\bar{\nu}_e$ CC selection:		
Kinematic tagging of e^+	98.6 %	1.1 %
Muon veto on tagged e^- and e^+	97.2 %	15.2 %
m_{+-} and ECAL on tagged e^+	93.2 %	30.9 %
TR + dE/dx on tagged e^+	83.8 %	99.2 %
RHC ν_e CC selection:		
Kinematic tagging of e^-	97.7 %	2.3 %
Muon veto on tagged e^+ and e^+	95.6 %	11.9 %
m_{+-} and ECAL on tagged e^-	91.1 %	29.7 %
TR + dE/dx on tagged e^-	82.0 %	99.3 %
FHC $\bar{\nu}_e$ CC selection:		
Kinematic tagging of e^+	98.4 %	0.3 %
Muon veto on tagged e^- and e^+	97.4 %	2.4 %
m_{+-} and ECAL on tagged e^+	93.7 %	6.0 %
TR + dE/dx on tagged e^+	84.3 %	93.6 %

docdb-13262

ν-H interaction sample

- ν-H scattering is free from **nuclear**
- STT allows the precise determination of the interaction target material (CH_2 vs C)
- Separation of ν-H from ν-C in (CH_2 target) with simple **kinem. and topological selections**

5y (FHC) + 5y (RHC)	Eff.	Purity	Size
ν_μ CC inclusive	93%	93%	2.9M
$\nu_\mu p \to \mu^- p \pi^+$	96%	95%	2M
$\nu_\mu p \to \mu^- p \pi^+ X$	89%	93%	760k
$\nu_\mu p \to \mu^- \pi^+ \pi^+ X$	75%	70%	93k
$\bar{\nu}_\mu$ CC inclusive	80%	84%	1.6M
$\bar{\nu}_\mu p \to \mu^+ n$	75%	80%	860k
$\bar{\nu}_\mu p \to \mu^+ p \pi^-$	94%	95%	300k
$\bar{\nu}_\mu p \to \mu^+ n \pi^0$	84%	84%	210k
$\bar{\nu}_\mu p \to \mu^+ p \pi^- X$	85%	94%	135K
$\bar{\nu}_\mu p \to \mu^+ n \pi \pi X$	82%	84%	156k

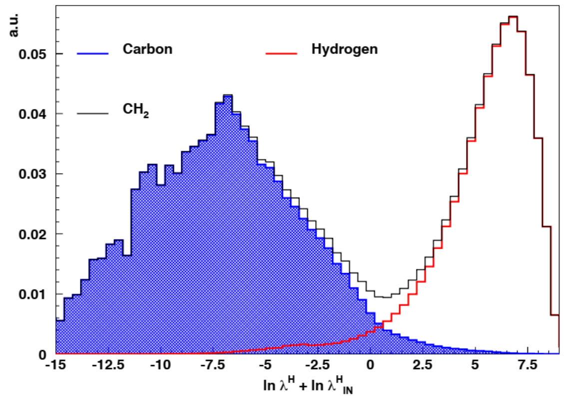

- Improvements exploiting the correlation of kinematical variables through the ratio of **multidimensional likelihoods**
- Possibility to study **exclusive channels**

[G. Ingratta]

docdb-13262

Flux Measurements

- SAND is well suitable to fully characterize $\nu(\bar{\nu})$ flux.
- ν_μ spectrum from low-ν sample [560k ev.] of
$$\nu_\mu + p \rightarrow \mu^- + p + \pi^+$$
- $\bar{\nu}_\mu$ spectrum from low-ν sample [610k ev.] of
$$\bar{\nu}_\mu + p \rightarrow \mu^+ + n$$
- ν_μ/ν_e and $\bar{\nu}_\mu/\bar{\nu}_e$ from reco ν_μ/ν_e CC scattering on H
- Absolute ν_μ flux from νe scattering [~1k ev./y]
- Additionally, $\bar{\nu}_\mu$ flux from $\bar{\nu}_\mu + p \rightarrow \mu^+ + n$ with $Q^2 < 0.05\ GeV^2$ [27k ev./y]

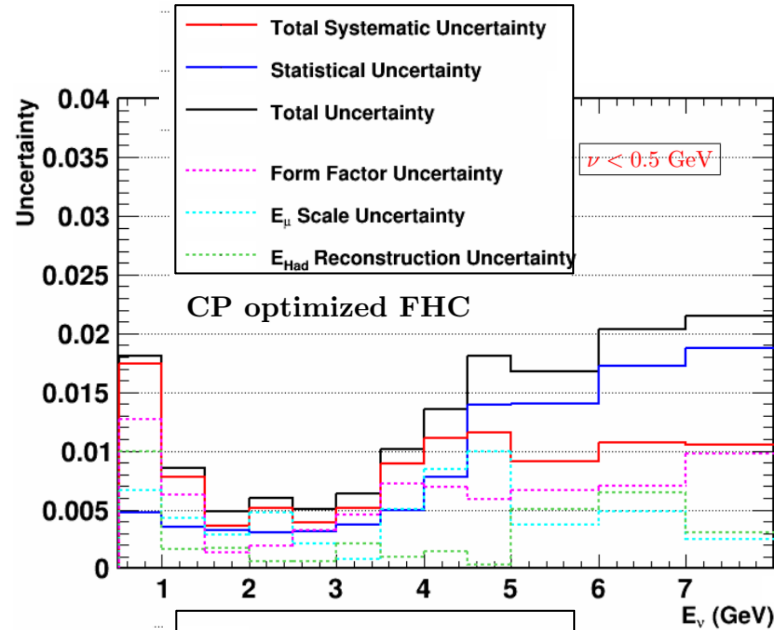

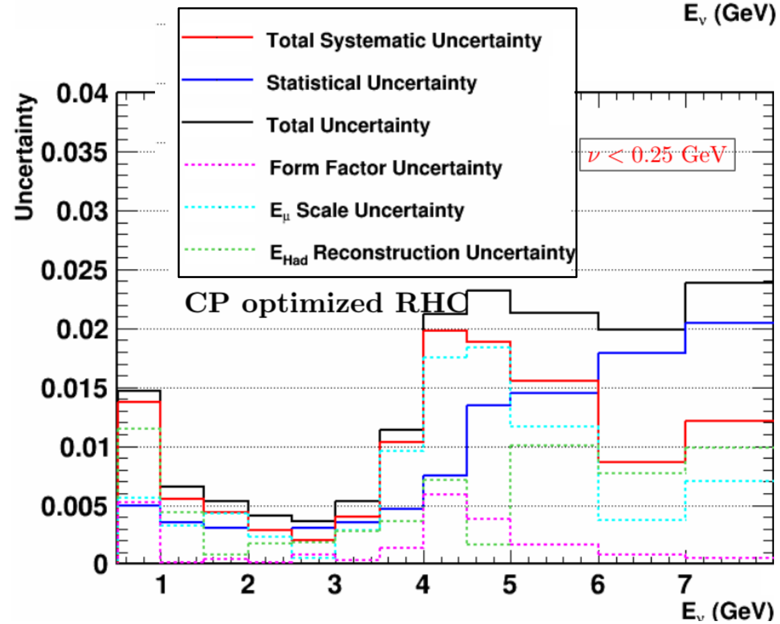

Beam Monitoring

Beam parameter	Variation	ECAL $\Delta\chi^2(E_\nu)$ true	ECAL $\Delta\chi^2(E_\nu)$ rec	ECAL $\Delta\chi^2(E_\mu)$ true	ECAL $\Delta\chi^2(E_\mu)$ rec
Horn current	+3 kA	107.6	76.1	26.0	25.4
Water layer thickness	+0.5 mm	21.2	16.2	8.7	8.5
Decay pipe radius	+0.1 m	42.0	34.3	12.0	11.9
Proton target density	+2%	18.0	14.3	8.9	8.7
Proton beam radius	+0.1 mm	34.9	27.6	18.2	17.8
Proton beam offset X	+0.45 mm	24.6	16.9	9.0	8.7
Proton beam θ, ϕ	0.07 mrad θ, 1.57 ϕ	0.5	0.1	0.1	0.1
Proton beam θ	0.070 mrad	0.7	0.2	0.1	0.1
Horn 1 X shift	+0.5 mm	16.2	10.7	4.3	4.1
Horn 1 Y shift	+0.5 mm	20.6	13.6	5.7	5.5
Horn 2 X shift	+0.5 mm	0.4	0.2	0.1	0.1
Horn 2 Y shift	+0.5 mm	0.4	0.1	0.0	0.0

Continuous beam monitoring on a weekly basis ($3.78 \times 10^{19}\ pot$) is crucial

A sample of **~780k** ν_μ CC events in the upstream barrel ECAL

Sensitivity on a list of possible variations obtained comparing expected spectra with:

$$\Delta\chi^2 = \sum_{i=1}^{N} \frac{(N_i^{\text{nom}} - N_i^{\text{var}})^2}{N_i^{\text{nom}}}$$

Beam direction monitoring: SAND can detect shifts down to 8.4 cm with a significance $\Delta\chi^2 \geq 9$

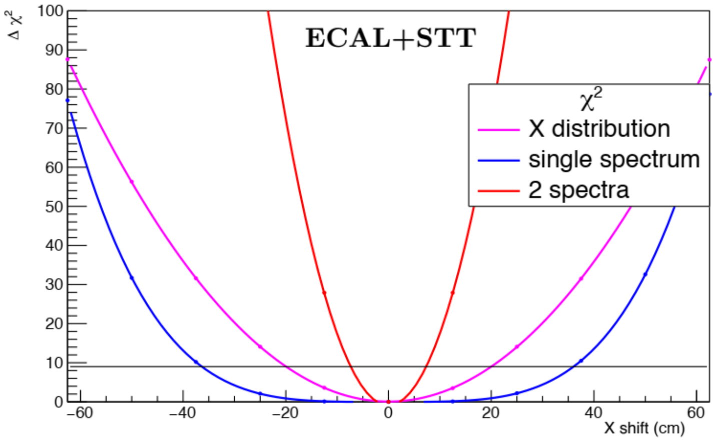

docdb-13262

[F. Barillari]

docdb-13262

External Background

- Backgrounds sources: CR, natural radioactivity and **products of external beam-neutrino interactions.**
  [first two bkg. suppressed to negligible level requiring beam spill coincidence].
- Several case studies for the 3rd source:
  - **Neutron Background in $\bar{\nu}_\mu + p \rightarrow \mu^+ + n$:** ANN with kinematical variables assigns rank to each isolated energy deposit (neutron candidate). The highest rank neutron candidate is the primary neutron in 85% and a secondary neutron in 6.5%
  - **Neutron Background in Inclusive $\nu(\bar{\nu})$ CC**: signal efficiency of 85.6% with a background rejection factor of 6 × 10−3
  - **Rock Muons and Magnet Events in Upstream ECAL:** Rejection factor is about 7×10−5. Overall efficiency of about 70% in the fiducial volume of the upstream barrel ECAL
  - **Rejection of External Neutrino Interactions in STT** : Overall we achieve a combined rejection factor of 3 × 10−5 against CC+NC external background, retaining a signal efficiency of 92.7% and a purity of 99.65%.
  - **Pile-up Background in Upstream barrel ECAL**: The fraction of CC events within the fiducial volume of the upstream barrel ECAL is 2.6% with the 30ns window.. The fraction of ECAL cells with pileup and the fraction of the pileup energy is 0.1% and 0.04% respectively with the 30ns window

ν_μ CCQE in GRAIN

[V. Cicero]

- Assess the contributions SAND (with GRAIN) could provide in understanding the physics of $\nu_\mu - Ar$ interactions
- The performances of SAND in terms of selecting exclusive $\mu^- + p$ are studied
- GRAIN exploited as homogeneous calorimeter
- CCQE-like selection has been defined:
  - Efficiency > 10% and Purity > 90%

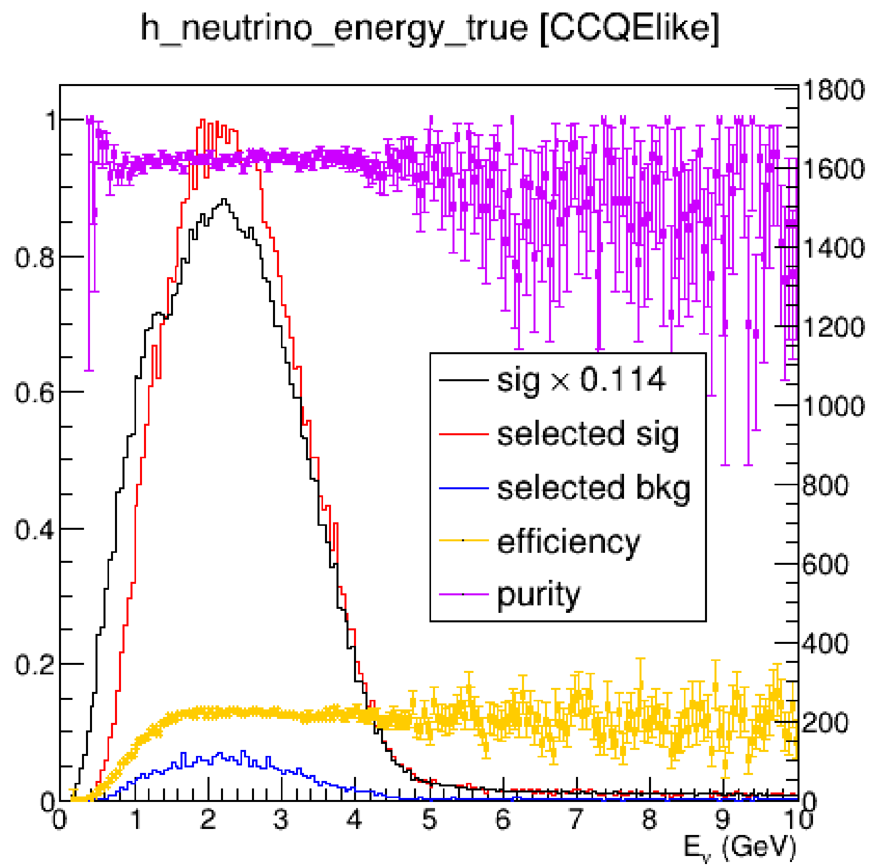

Next steps

- We have obtained the previous results (docdb-13262) mainly using the fast reconstruction
- The main goal, now is to develop a **full reconstruction**
- In order to **reproduce the analyses** w/ full reconstruction

Ongoing activities

- Implement and optimize a full event reconstruction **[F. Alemanno, A. Surdo]**
- Comparison of straw- VS drift-based tracker using same reconstruction tools **[M. Sorbara, A. Gioiosa]**
- ECAL:
  - Integrate new endcap geometry in sandreco **[P. Gauzzi, A. Ruggeri]**
  - Assess PID performances **[D. Casazza, R. D’Amico]**
- Assess beam monitoring potential with more realistic reconstruction **[F. Barilari]**
- Analysis:
  - Study νH in a exclusive channel: $\bar{\nu}_\mu + p \rightarrow \mu^+ + n$ **[G. Ingratta]**
  - Study ν CCQE in GRAIN with exclusive topology: $\mu + p$ **[V. Cicero]**

Kalman Filter

Kalman Filter

[V. Pia]

«Kalman filtering is an iterative algorithm that provides estimates of some unknown variables given the **measurements** observed over time»
(**state**)

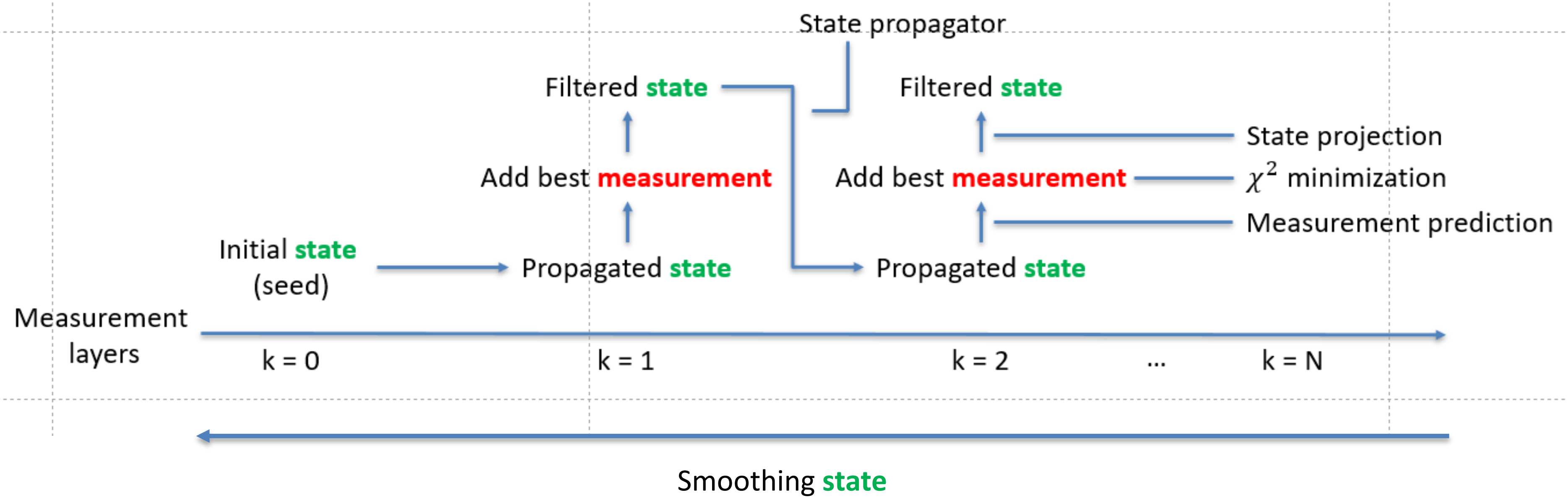

[dune / STTTrackReco · GitLab (infn.it)]

Trajectory Parametrization

- **Trajectory state vector (a_k)**

$$\begin{pmatrix} x \\ y \\ q/R \\ \tan\lambda \\ \phi \end{pmatrix}$$

- x → x coordinate
- y → y coordinate
- q/R → signed inverse radius
- $\tan\lambda$ → tangent of dip angle
- ϕ → rotation angle

- **Measurement vector (m_k)**

$$m_x = \begin{pmatrix} x \\ \theta_{xz} \end{pmatrix}$$ Angle in the horizontal plane wrt z-axis

$$m_y = \begin{pmatrix} y \\ \theta_{yz} \end{pmatrix}$$ Angle in the vertical plane wrt z-axis

- KF propagation from downstream to upstream

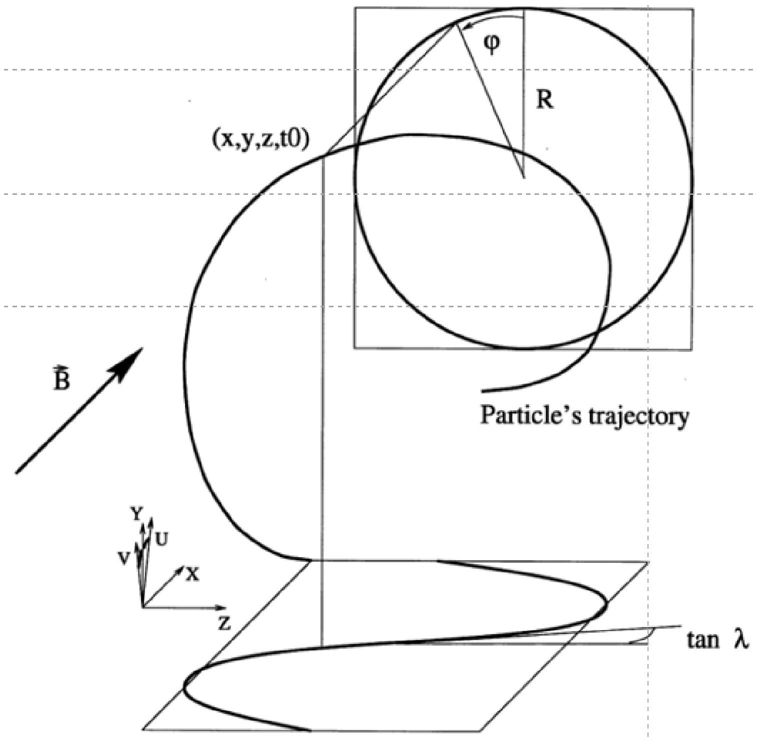

INFN Istituto Nazionale di Fisica Nucleare DUNE

Propagation

- State vector propagation from z_{k-1} *to* z_k

$$f_{k-1}: \quad \begin{aligned} x_k &= x_{k-1} + \tilde{R}_{k-1} \cdot \tan\lambda_{k-1} \cdot (\phi_k - \phi_{k-1}) \\ y_k &= y_{k-1} + R_{k-1} \cdot (\sin\phi_k - \sin\phi_{k-1}) \\ 1/\tilde{R}_k &= 1/\tilde{R}_{k-1} + \kappa \cdot \Delta(1/R_{k-1}) \\ \tan\lambda_k &= \tan\lambda_{k-1} \\ \cos\phi_k &= \cos\phi_{k-1} + (z_k - z_{k-1})/R_{k-1} \end{aligned}$$

$$\Delta(1/R) = -\frac{(1/R)^2}{0.3 \cdot B} \cdot \sqrt{1+\tan^2\lambda} \cdot \sqrt{1 + \frac{m^2(1/R)^2}{(0.3 \cdot B)^2}(1+\tan^2\lambda)} \cdot \Delta E$$

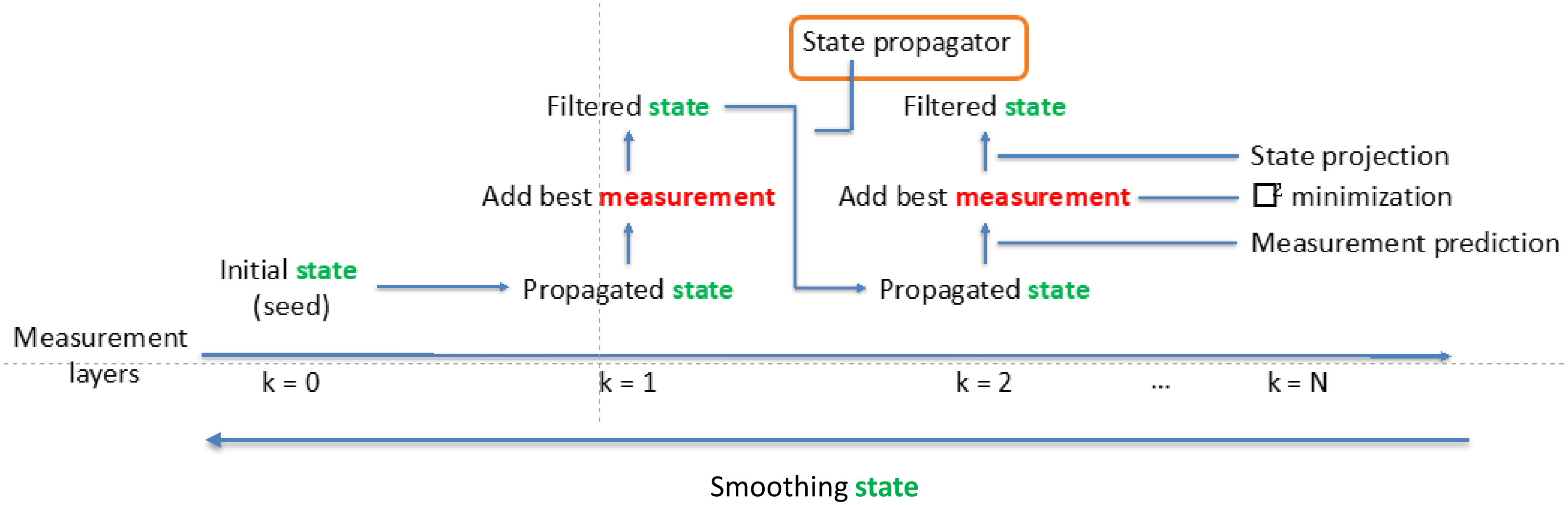

Projection

Prediction of measurement vector m_k from propagated state vector

$$h_k^{(x)} = \begin{pmatrix} x_k \\ -q \cdot \arctan \dfrac{\tan \lambda_k}{\sin \phi_k} \end{pmatrix}$$

$$h_k^{(y)} = \begin{pmatrix} y_k \\ \phi_k + q \cdot \dfrac{\pi}{2} \end{pmatrix}$$

Measurement projection to state vector

$$H_k^{(x)} = \begin{pmatrix} 1 & 0 & 0 & 0 & 0 \\ 0 & 0 & 0 & \dfrac{\kappa}{\sin \phi_k \cdot \left[1+\left(\frac{\tan \lambda_k}{\sin \phi_k}\right)^2\right]} & -\dfrac{\tan \lambda_k}{\tan \phi_k} \cdot \dfrac{\kappa}{\sin \phi_k \cdot \left[1+\left(\frac{\tan \lambda_k}{\sin \phi_k}\right)^2\right]} \end{pmatrix}$$

$$H_k^{(y)} = \begin{pmatrix} 0 & 1 & 0 & 0 & 0 \\ 0 & 0 & 0 & 0 & 1 \end{pmatrix}$$

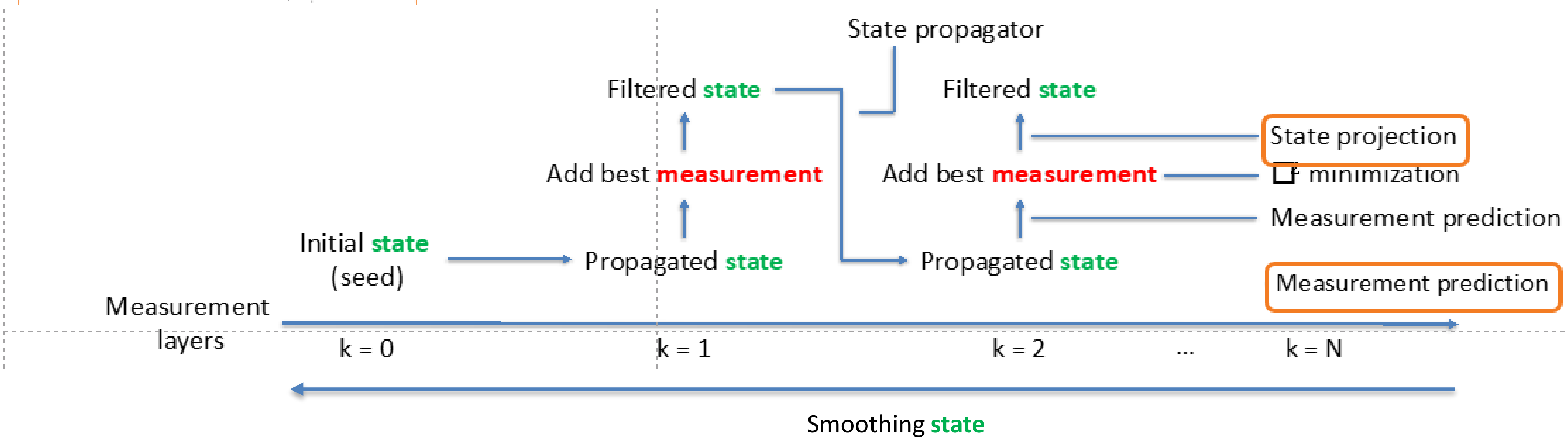

ΔE and MCS

Energy loss from layer *k-1* to layer *k* computed as:

$$\Delta E_k = \left.\frac{dE}{dx}\right|_{Bethe-Bloch} \times \Delta Z_k \; [g \cdot cm^{-2}]$$

$$\Delta Z_k = \rho \cdot L \left[\frac{g}{cm^2}\right]$$

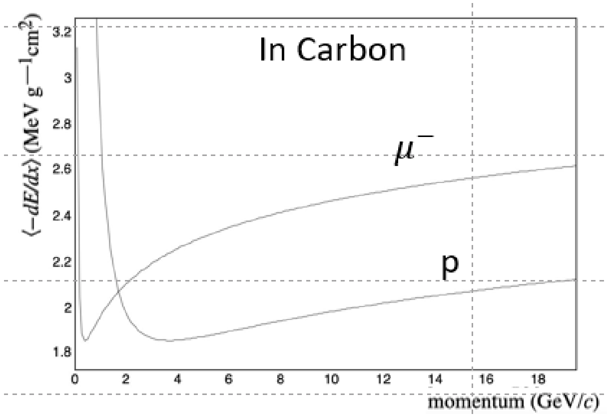

MCS angle computed as:

$$\theta_k = \frac{13.6\ \text{MeV}}{\beta c p} \cdot q \cdot \sqrt{\Delta Z_k / X_0}\,[1 + 0.038 \ln(\Delta Z_k / X_0)]$$

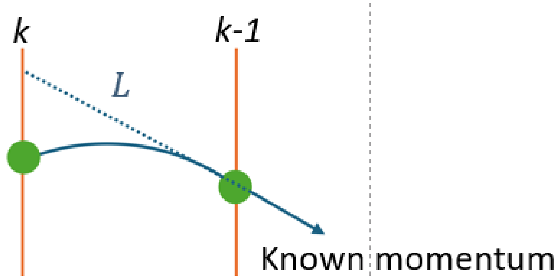

Where:

- materials information taken from geometry file
- L computed as a straight line from measurement layer *k-1* to *k*
- direction taken from trajectory state of previous step

Caveats for KF validation

$$\Delta(1/R) = -\frac{(1/R)^2}{0.3\cdot B}\cdot\sqrt{1+\tan^2\lambda}\cdot\sqrt{1+\frac{m^2(1/R)^2}{(0.3\cdot B)^2}(1+\tan^2\lambda)}\cdot\Delta E$$

$$m_x = \binom{x}{\theta_{xz}}$$

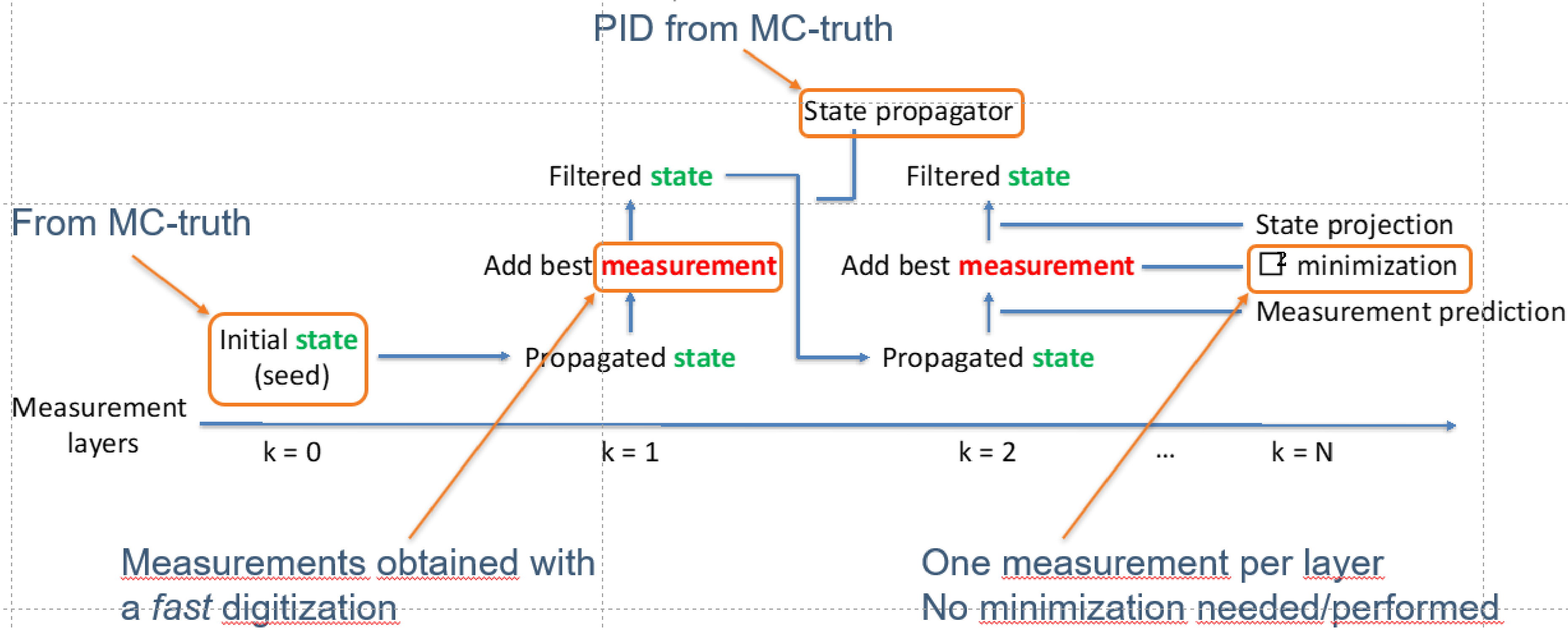

Simulation chain

SAND Geometry
- GDML file as seen earlier

Neutrino Flux
- LBNF beam flux (same as for DUNE TDR)

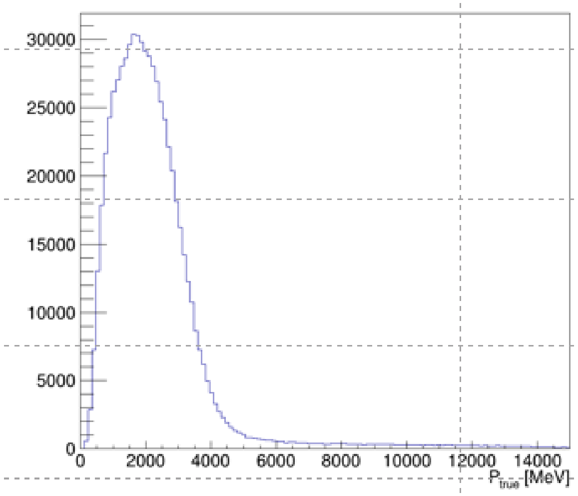

Genie Production
- ν_μ CC in SAND tracker

Particle propagation
- EDepSim (Geant4 wrapper)

Track selection
- μ^-, π^+, p produced at vertex

Digitization
- Fast simulation

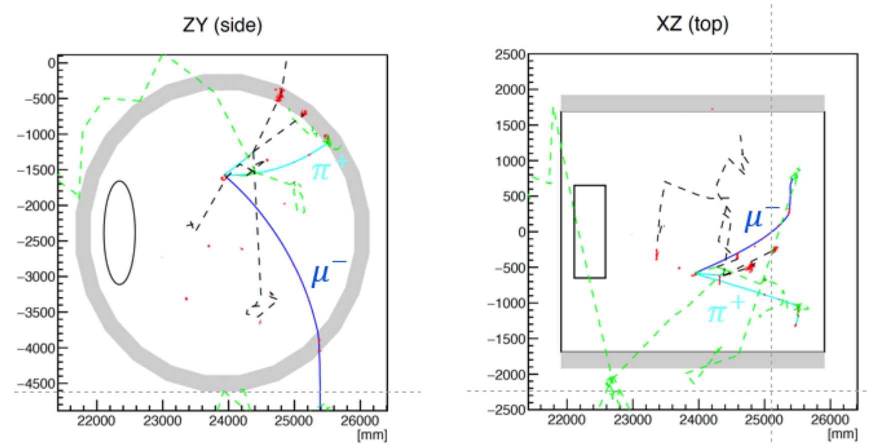

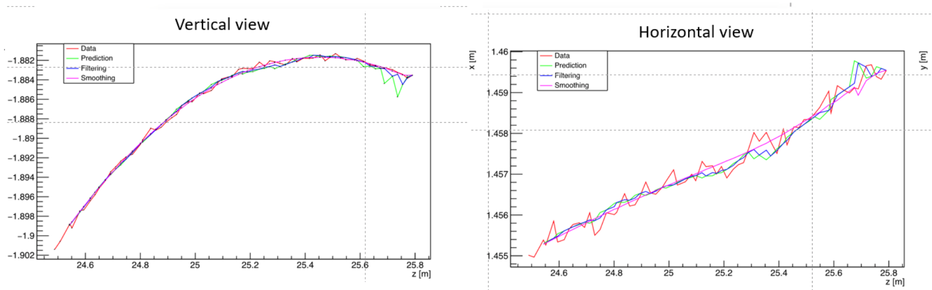

KF Validation [WIP]

$$r_k = m_k^{pred} - m_k^{true}$$

$$C_k = \text{ covariance matrix}$$

- Two consistency checks:

1. $q_k = r_k^T C_k^{-1} r_k \sim \chi^2(ndf = 2)$

2. $g(i)_k = \frac{r(i)_k}{\sqrt{C(i)_k}} \sim Gaus(\mu = 0, \sigma = 1)$

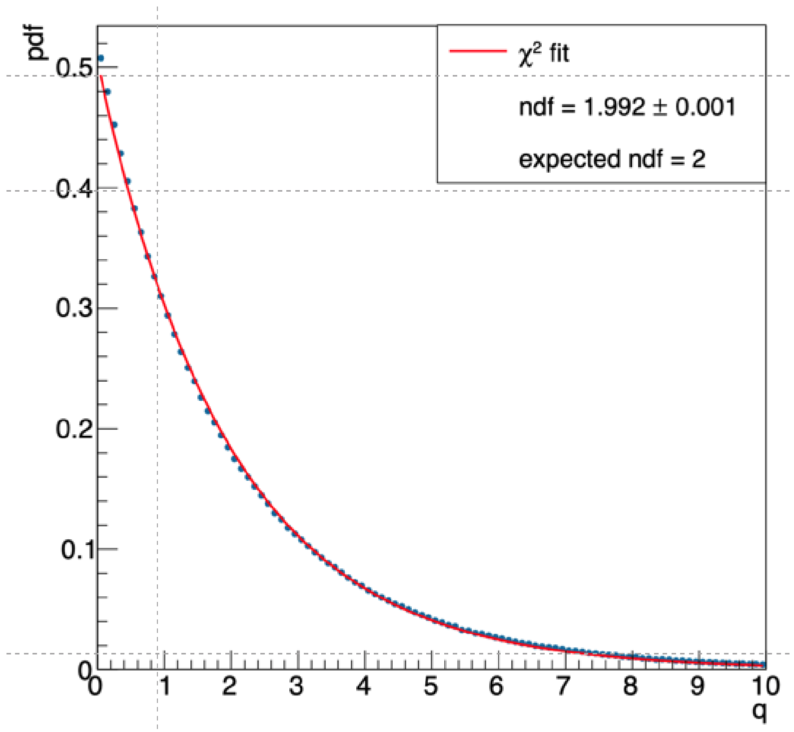

KF Validation [WIP]

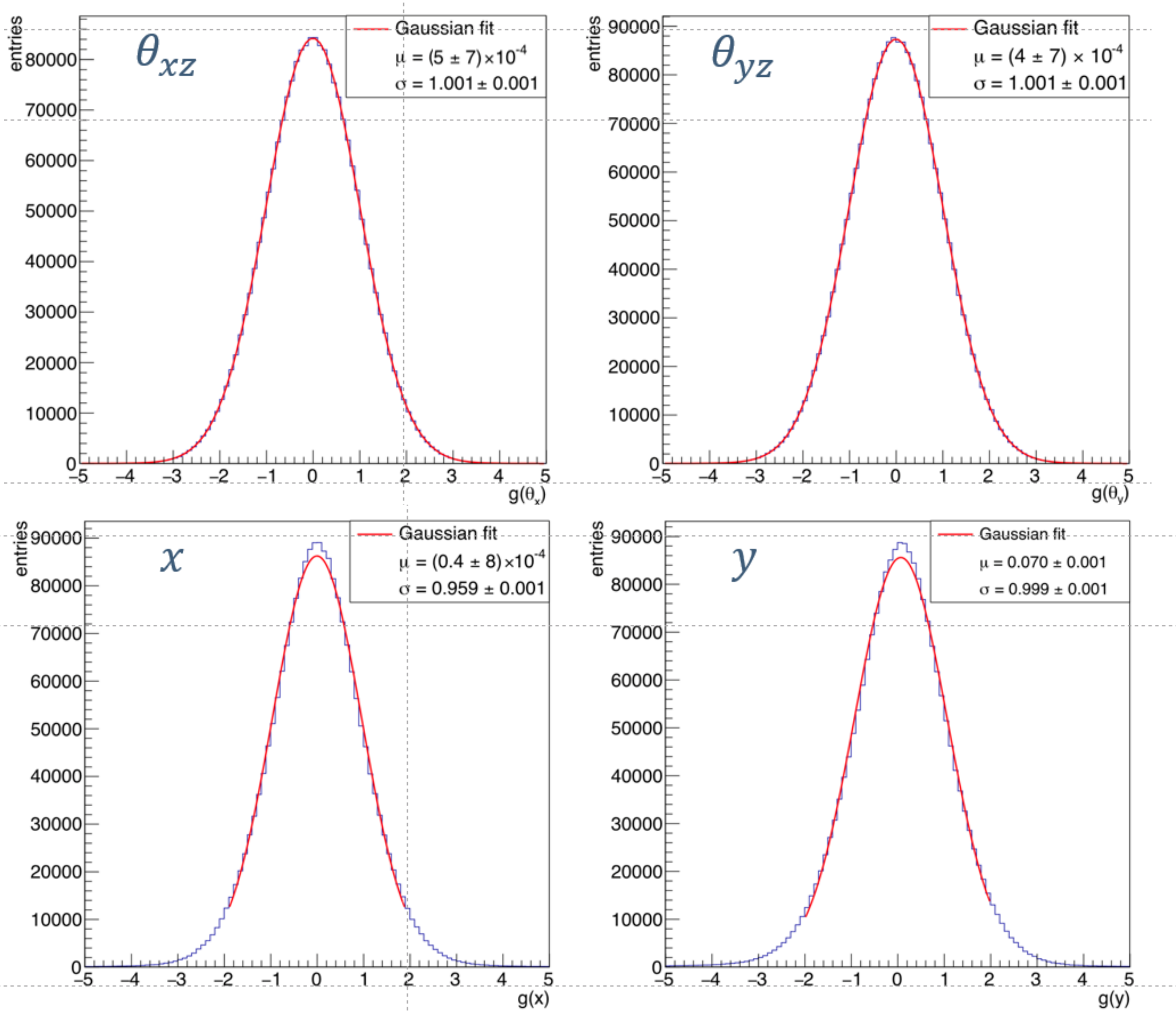

$$g(\theta)_k = \frac{r(\theta)_k}{\sqrt{C(\theta)_k}}$$

$$g(pos)_k = \frac{r(pos)_k}{\sqrt{C(pos)_k}}$$

ECAL clustering

Reconstruction of energy deposit position, time and energy

The coordinate along the fiber z is derived by time difference between two ends while x and y are given by the center of the fired cell.

$$t^e = \frac{t^A + t^B}{2} - \frac{t_0^A + t_0^B}{2} - \frac{L}{2v} \qquad z^e = \frac{v}{2}\left(t^A - t^B - t_0^A + t_0^B\right)$$

$t^{A,B}$ time in ns measured at the ends, $t_0^{A,B}$ overall time offset, L length of the cell, v light velocity in the fiber.

Each cell is read by two photosensors, one per side (A,B) which collects the scintillation light guided by the optical fibers.

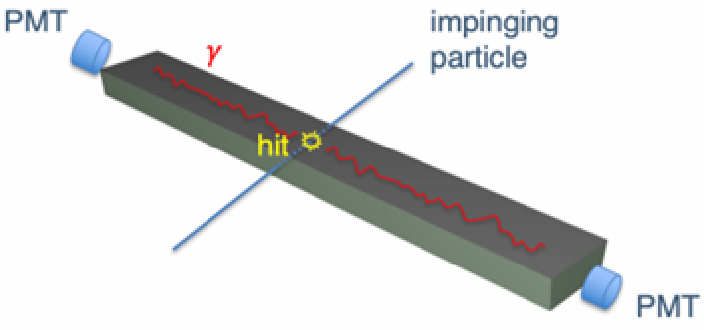

Clustering

C++ algorithm inspired by KLOE experiment to create ECAL cluster output as ROOT TTree

Cells are divided in **complete** (signal on both photo sensors) and **incomplete** (with signal only in one sensor).

Neighbor complete cells are grouped in pre-clusters.

- **Pre-clustering**

Takes one complete cell as a seed and checks the neighbors, if are found complete cells they are added to the pre-cluster.

The process goes on until no adjacent complete cells are found.

Pre-cluster variables are calculated, time and position as energy weighted averages over contributing cells, energy as the sum of the cell energies.

$$E_i = \frac{E_i^A + E_i^B}{2}$$

- **Splitting** compute time variance of the pre-cluster and in case of time discrepancy > 5ns divides into quadrants forming new pre-clusters.
- **Merging** compares two close pre-clusters and merges them if their spatial distance is < 40 cm and time difference < 2.5 ns.
- Adding incomplete cells to the pre-clusters, comparing cell position and closest pre-cluster centroid.

Under testing, validation and optimization

Thank you

Backup

ND sim/reco «official ND production»

- Infrastructure for production chain:
  - Event generator, detector responce simulation, digitization, reconstruction

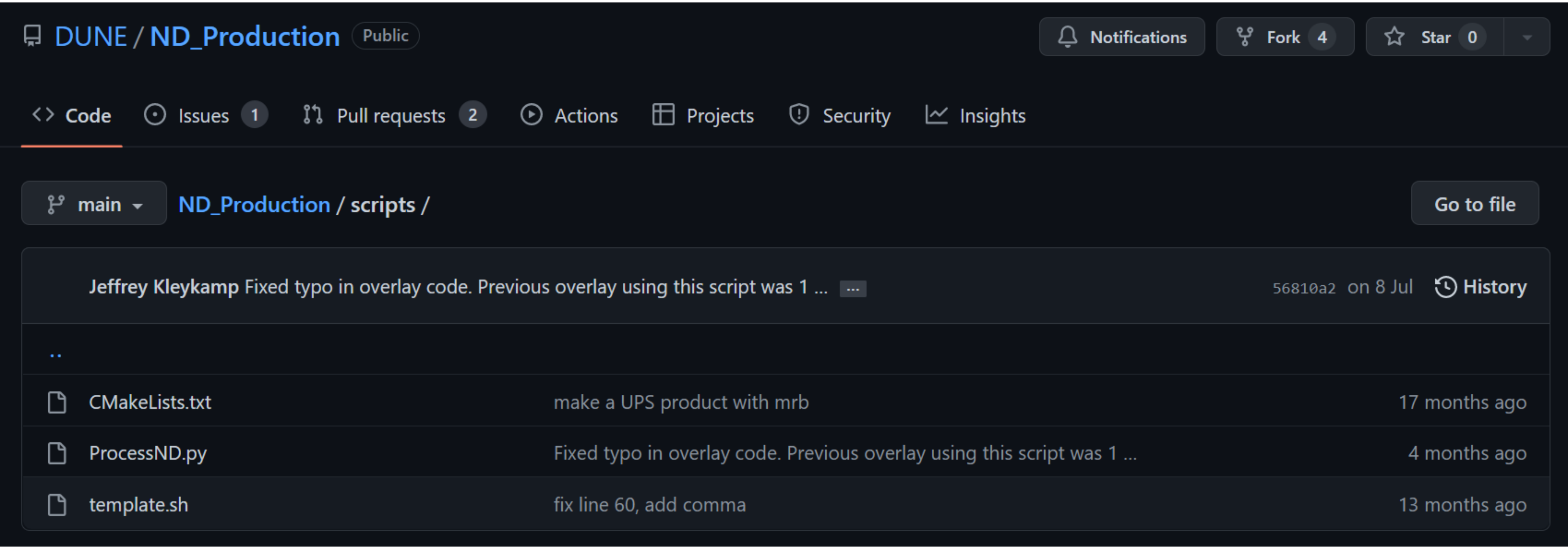

CAF Maker

- Common Analysis File
- Event Summary
- Input for Analyses
- SAND CAF implemented
- Content to be defined

DUNE / ND_CAFMaker Public

Notifications

Code | Issues 2 | Pull requests 1 | Actions | Projects | Security | Insights

master ▾ ND_CAFMaker / src / reco /

chenel whoops, don't be lazy. put implementation in .cxx

..

IRecoBranchFiller.h	Merge branch 'master' into feature/TMSconverer to pick up c
MLNDLArRecoBranchFiller.cxx	Merge branch 'master' into feature/TMSconverer to pick up c
MLNDLArRecoBranchFiller.h	getting rid of dt + parametrized reco
NDLArProductFiller.cxx	whoops, don't be lazy. put implementation in .cxx
NDLArProductFiller.h	whoops, don't be lazy. put implementation in .cxx
NDLArSummaryH5DatasetReader.cxx	quiet print statements in NDLAr fillers
NDLArSummaryH5DatasetReader.h	once again, don't set a size_t to -1 (eyeroll)
NDLArTMSMatchRecoFiller.cxx	Update matcher to use TMS distances in cm units, and not to convert L...
NDLArTMSMatchRecoFiller.h	Update matcher to slightly different method (propagate the LAr track ...
SANDRecoBranchFiller.cxx	Automatically enable or disable compilation of sand reco based on exi...
SANDRecoBranchFiller.h	Automatically enable or disable compilation of sand reco based on exi...
TMSRecoBranchFiller.cxx	Move TMS reco branches to have lengths in cm, not mm, as to match LAr...
TMSRecoBranchFiller.h	Merge branch 'master' into feature/TMSconverer to pick up changes due...

ECAL

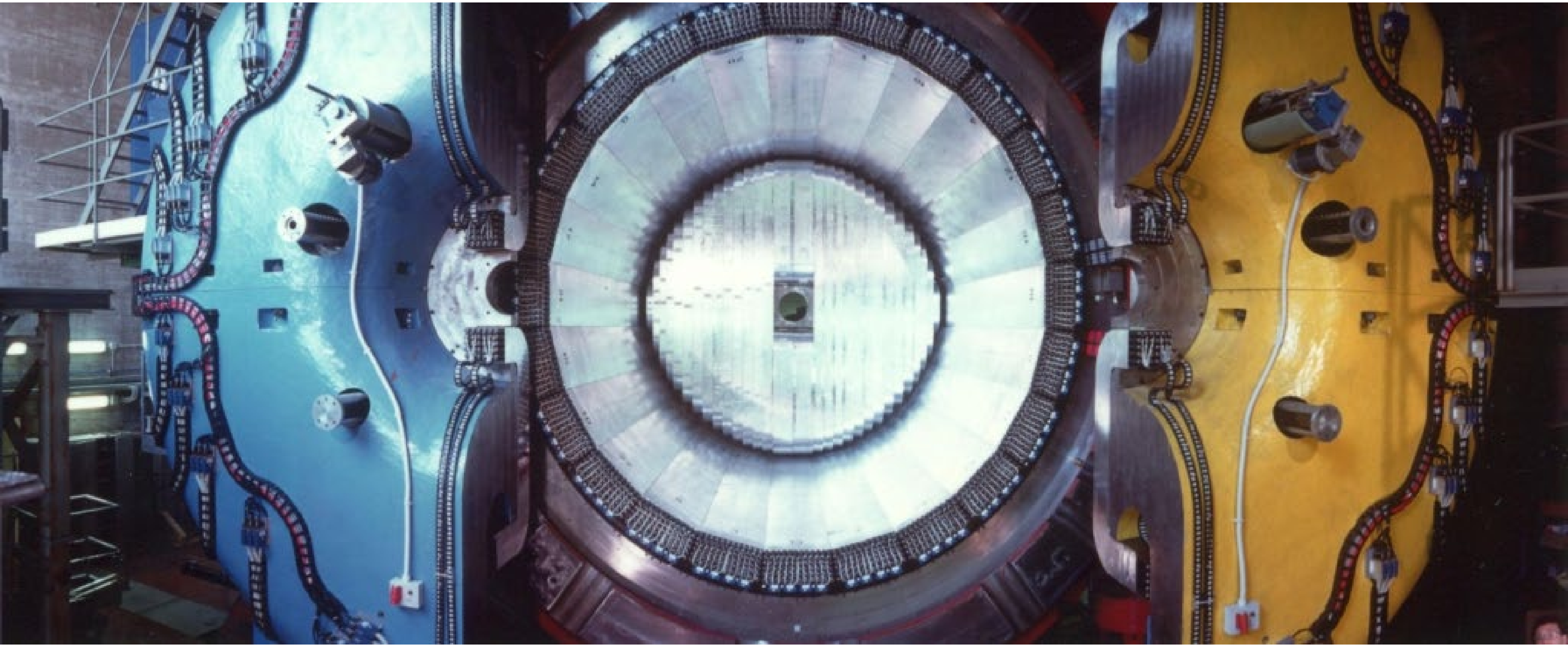

ECAL

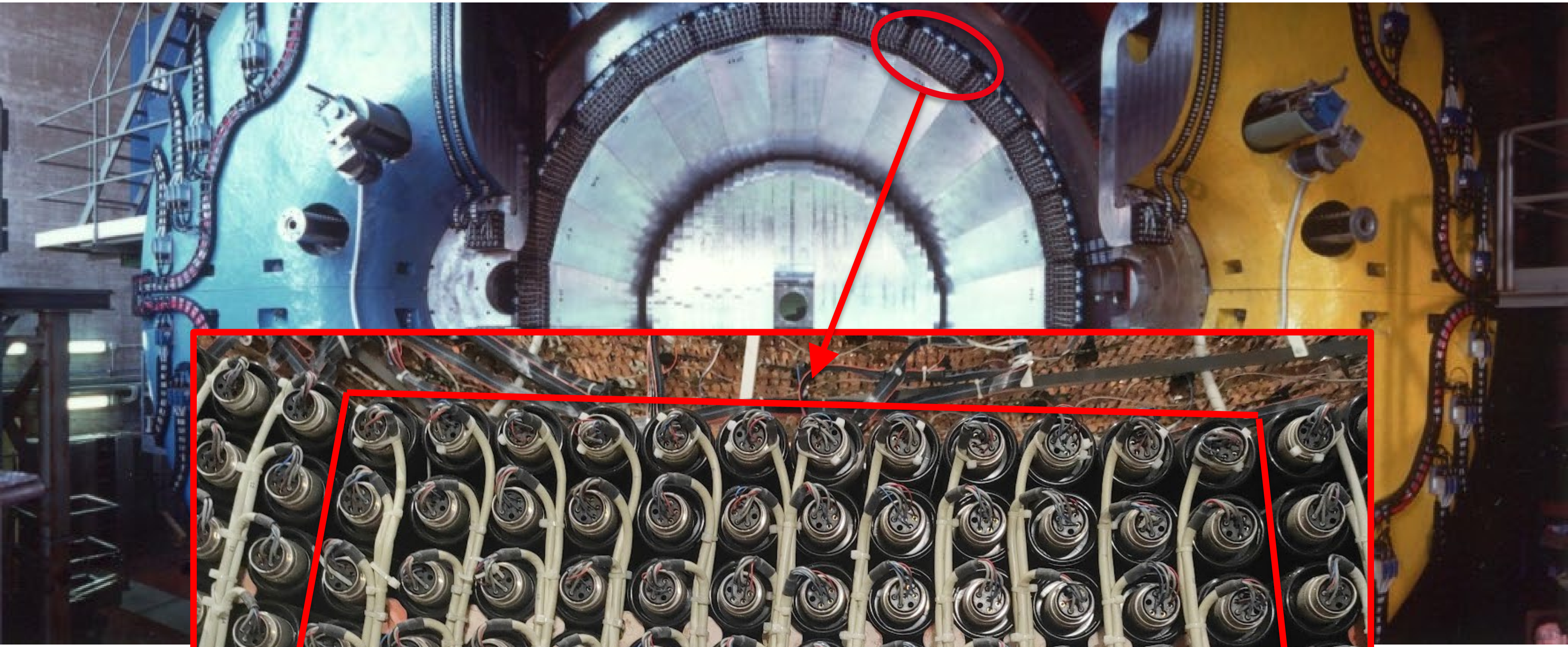


BAR 17
SIDE 2
CH 01:15
BAR 17
SIDE 2
CH 16:30
BAR 17
SIDE 2
CH 31:45
BAR 17
SIDE 2
CH 46:60

ECAL

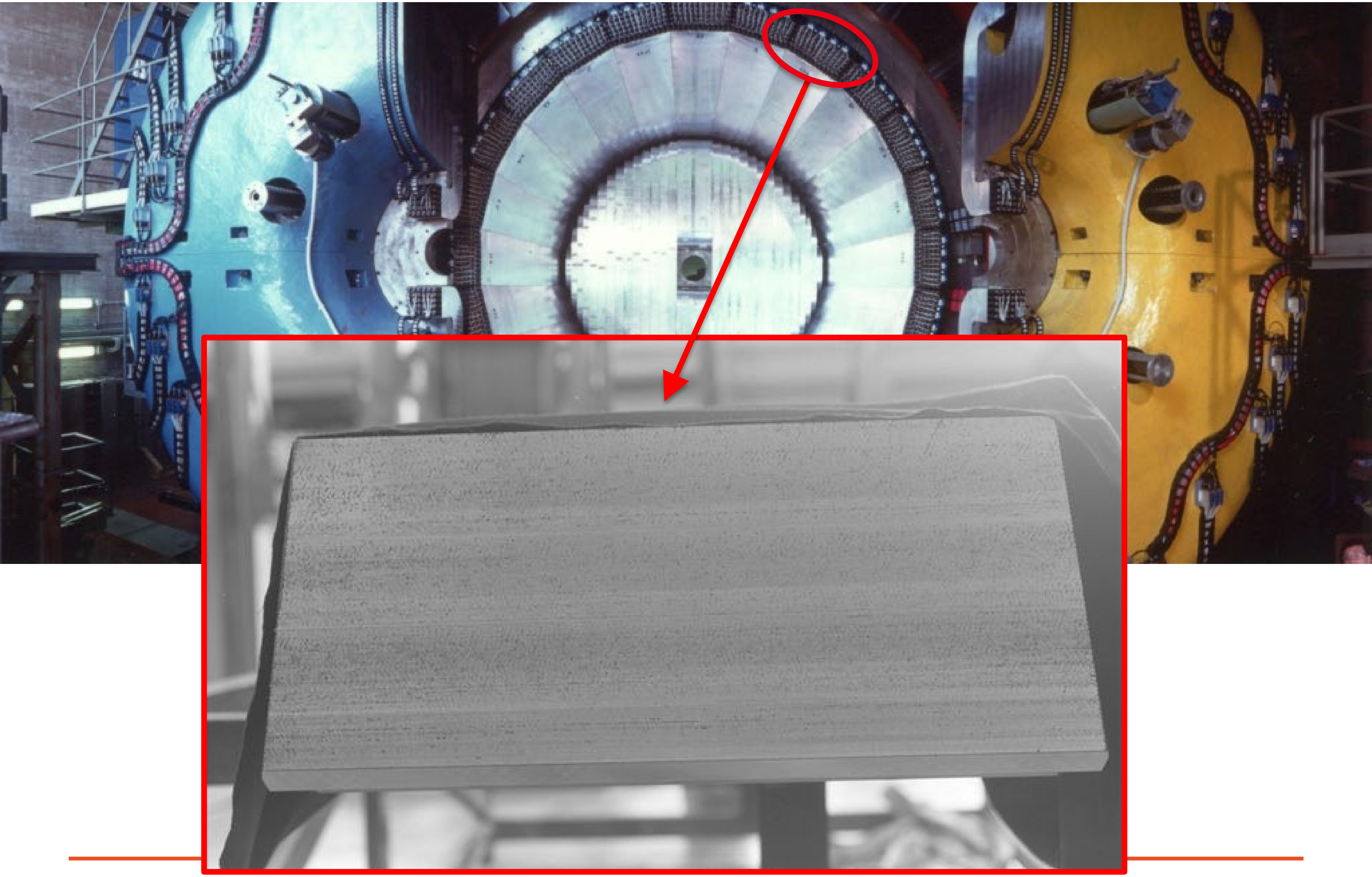

ECAL

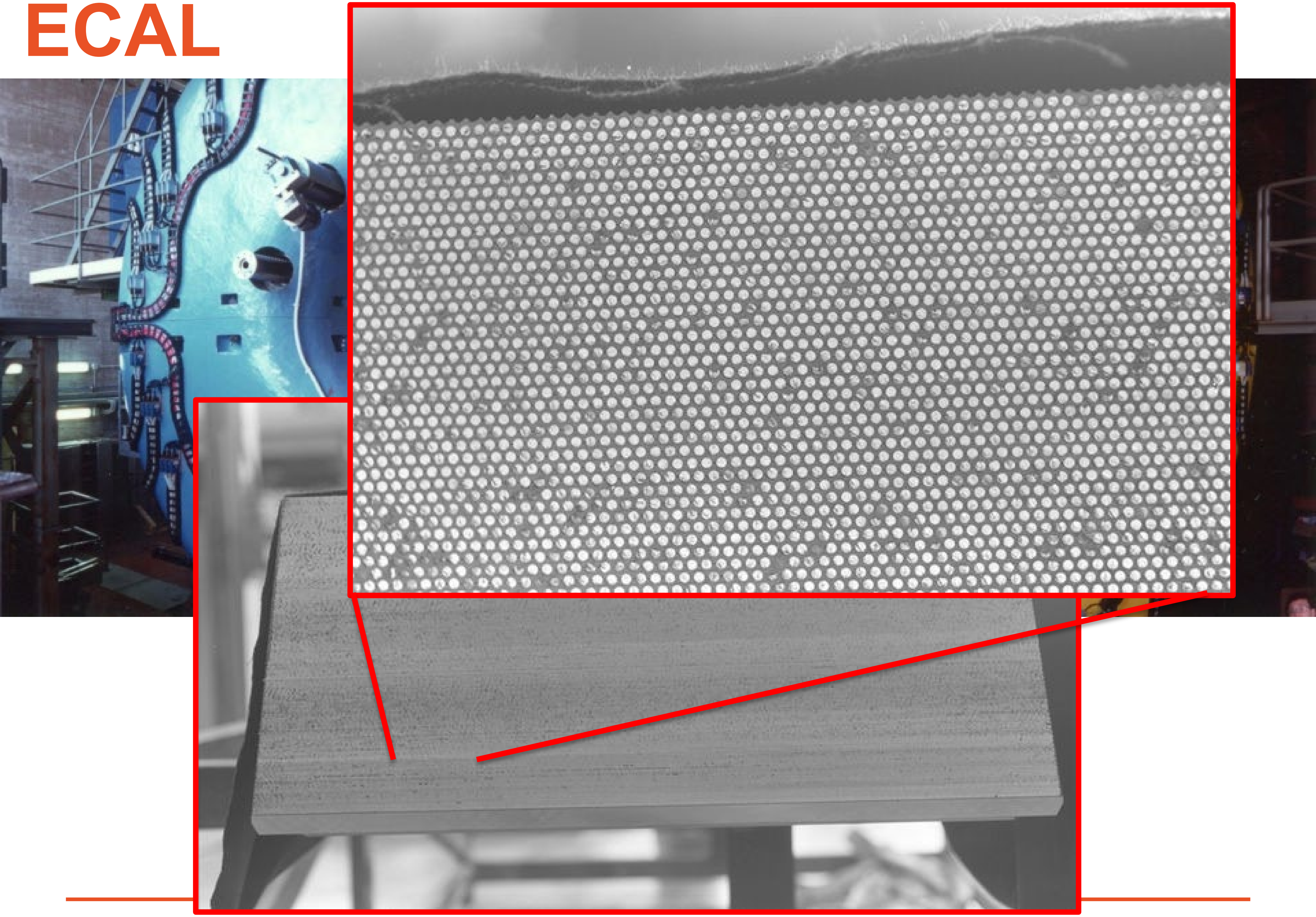

LAr Vessel Vacuum Sup Insulated

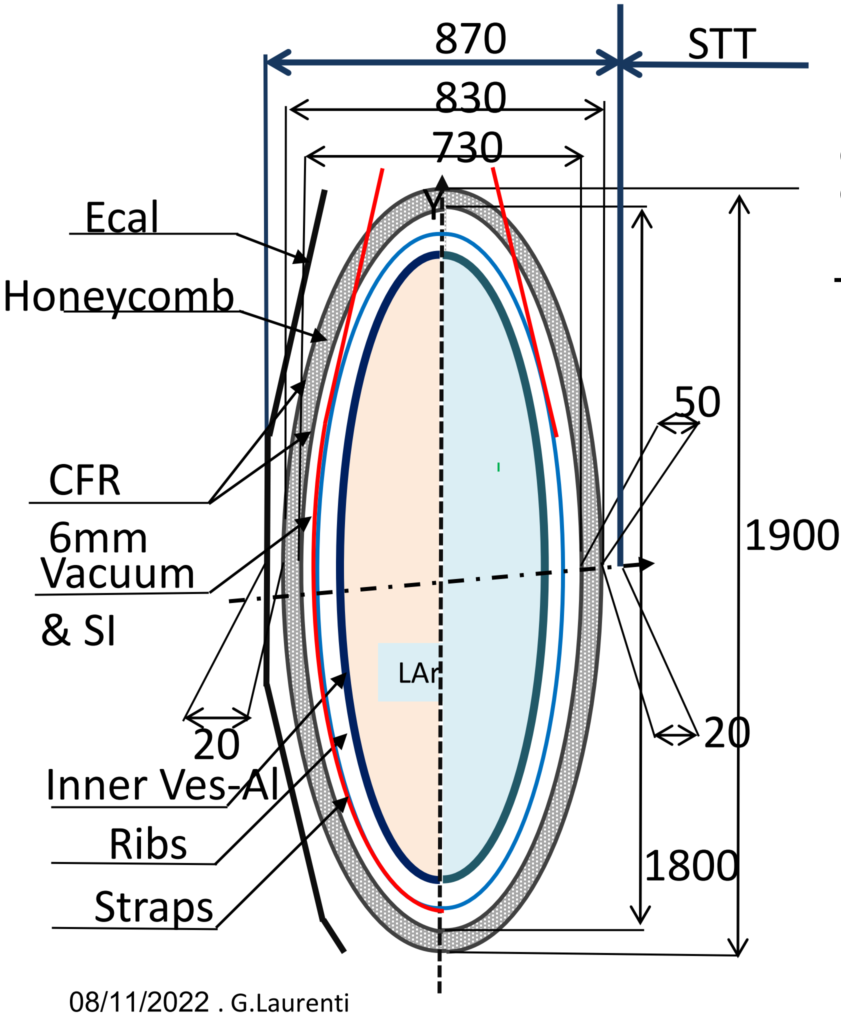

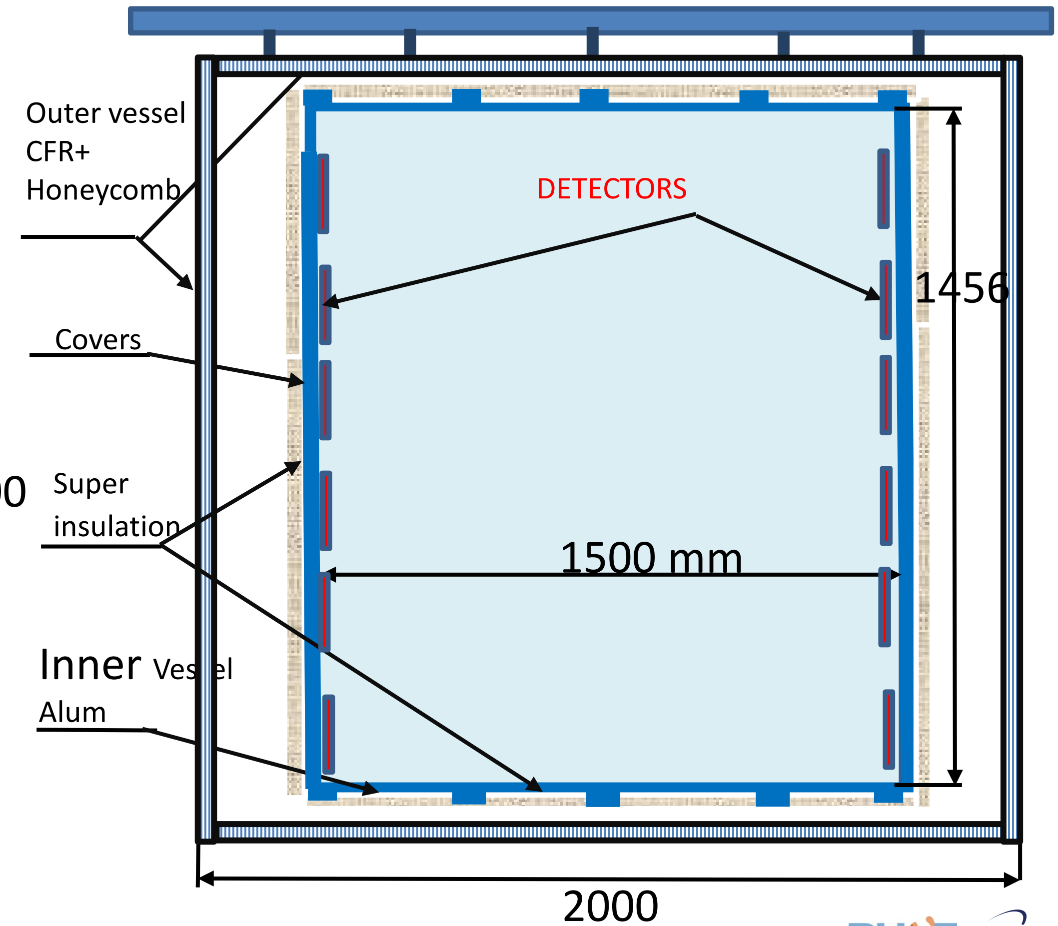

Internal vessel design

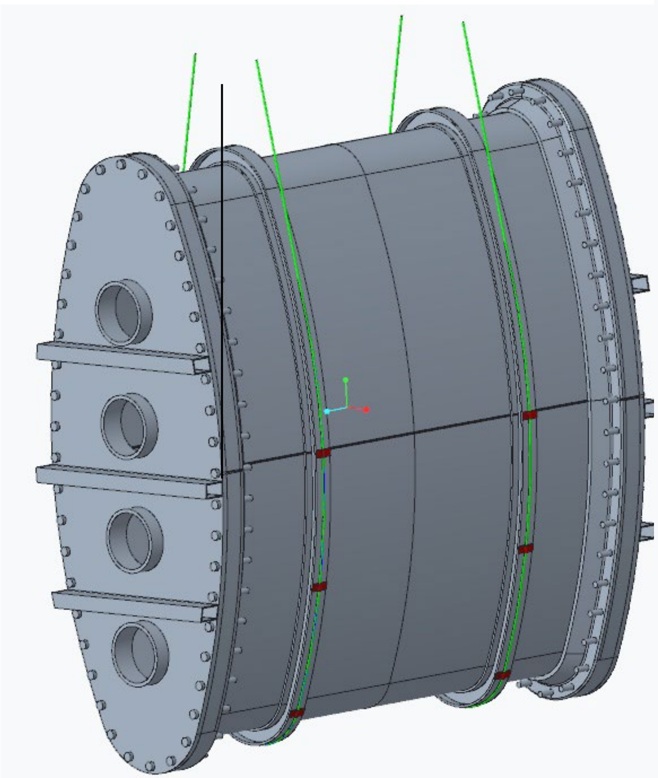

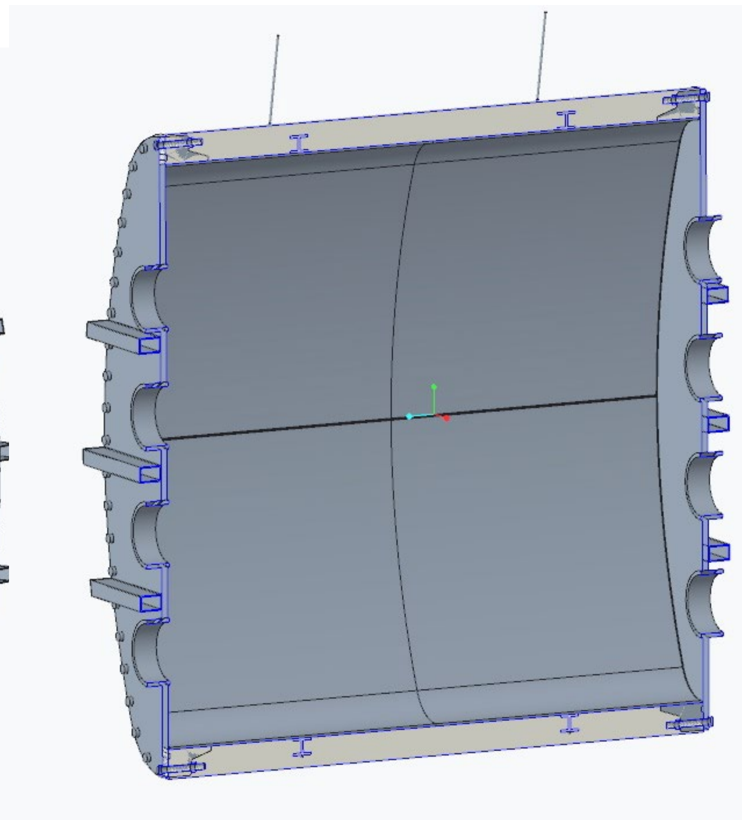

- Material AISI 316LN
- Internal pressure 1.5 bar
- Shell thickness 6 mm
- Cover thickness 16 mm

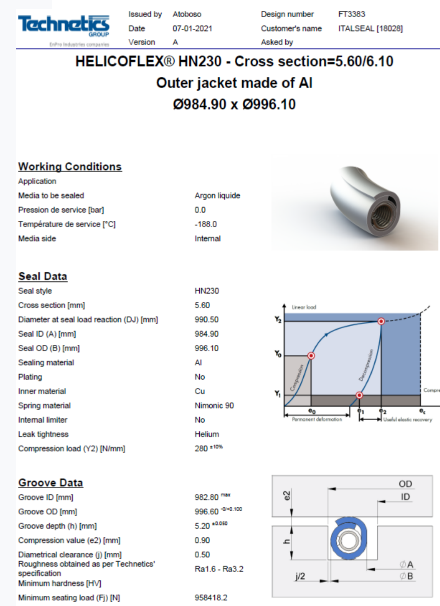

Technetics GROUP — EnPro Industries companies

Issued by	Atoboso	Design number	FT3383
Date	07-01-2021	Customer's name	ITALSEAL [18028]
Version	A	Asked by	

HELICOFLEX® HN230 - Cross section=5.60/6.10

Outer jacket made of Al

Ø984.90 x Ø996.10

Working Conditions

Application	
Media to be sealed	Argon liquide
Pression de service [bar]	0.0
Température de service [°C]	-188.0
Media side	Internal

Seal Data

Seal style	HN230
Cross section [mm]	5.60
Diameter at seal load reaction (DJ) [mm]	990.50
Seal ID (A) [mm]	984.90
Seal OD (B) [mm]	996.10
Sealing material	Al
Plating	No
Inner material	Cu
Spring material	Nimonic 90
Internal limiter	No
Leak tightness	Helium
Compression load (Y2) [N/mm]	280 $^{\pm 10\%}$

Groove Data

Groove ID [mm]	982.80 ^{max}
Groove OD [mm]	996.60 $^{-0/+0.100}$
Groove depth (h) [mm]	5.20 $^{\pm 0.050}$
Compression value (e2) [mm]	0.90
Diametrical clearance (j) [mm]	0.50
Roughness obtained as per Technetics' specification	Ra1.6 - Ra3.2
Minimum hardness [HV]	
Minimum seating load (Fj) [N]	958418.2

External vessel design

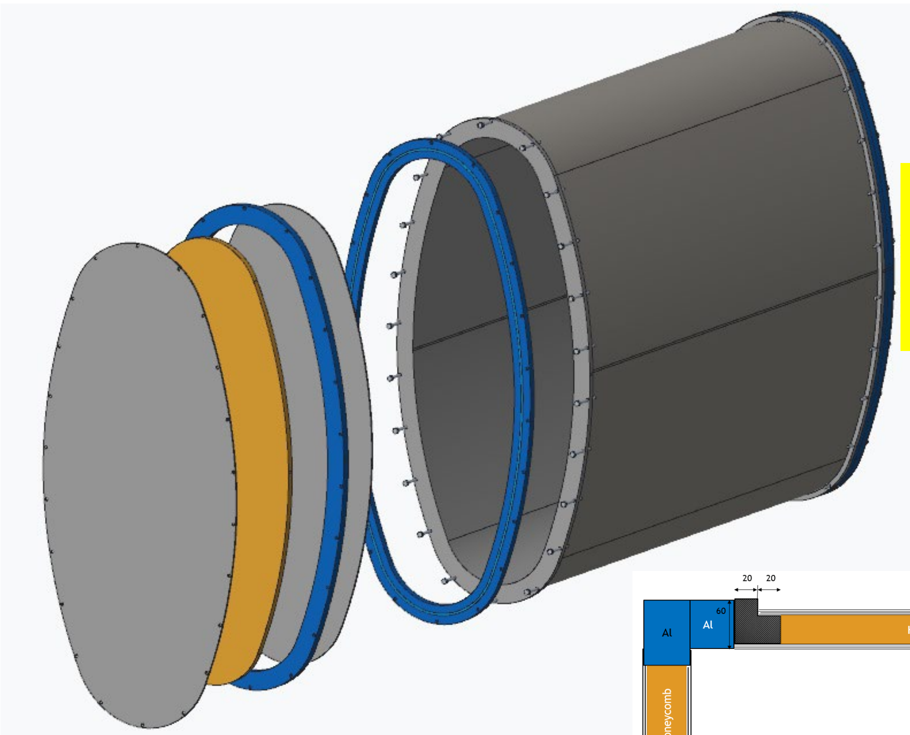

Aluminum alloy

Carbon fiber

Honeycomb

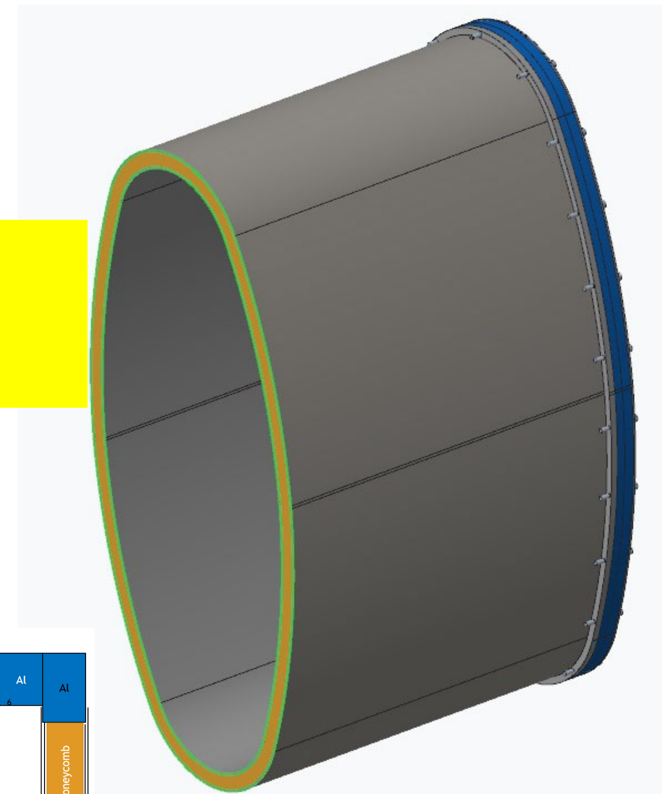

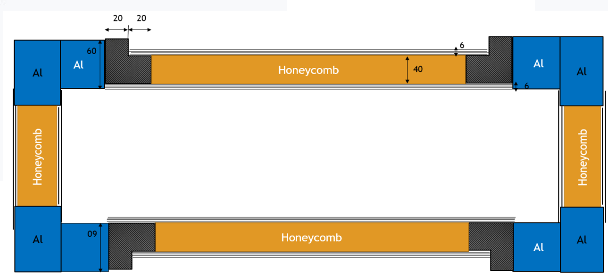

Optical System: Lens

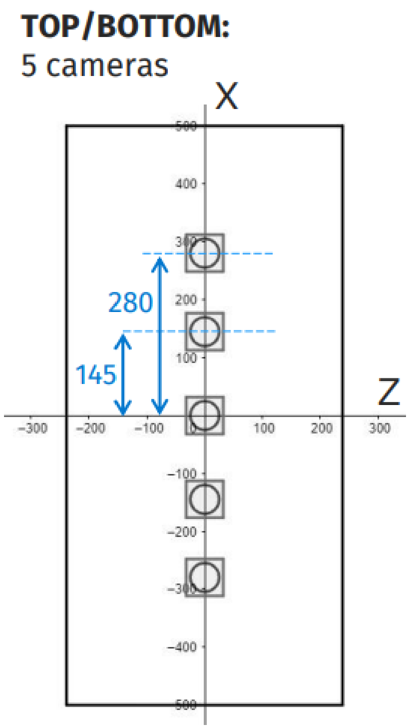

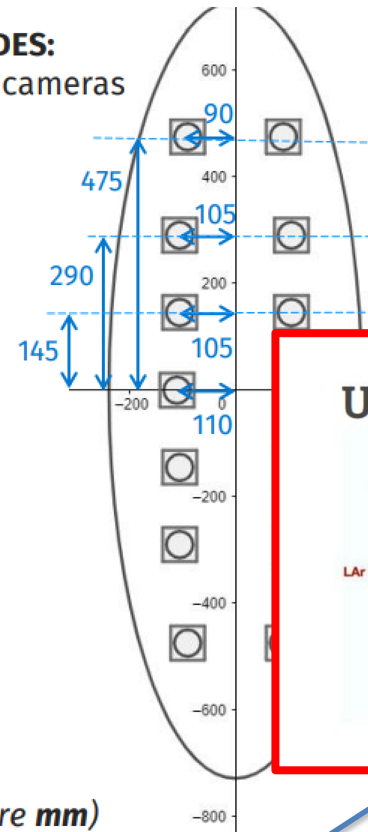

(*Units are **mm***)

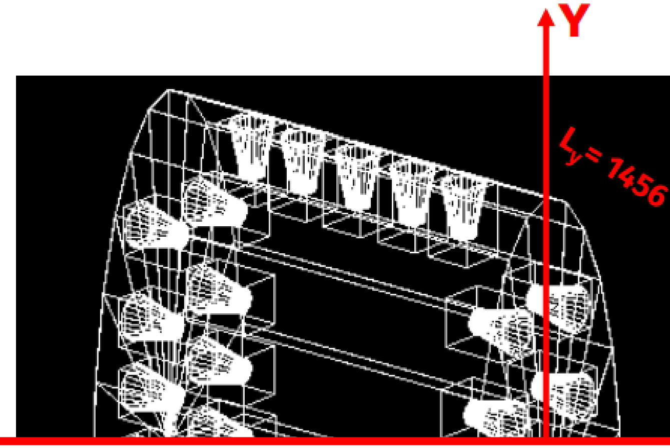

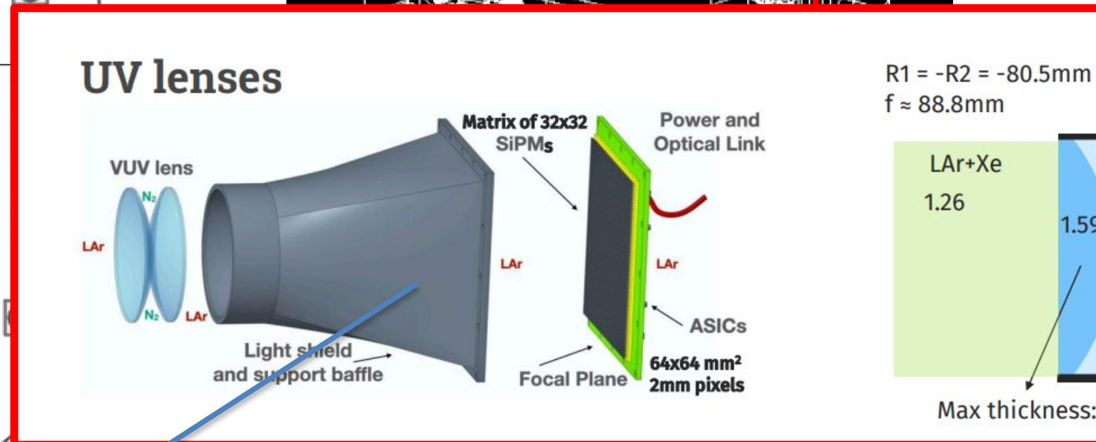

Optical System: Coded Aperture Mask

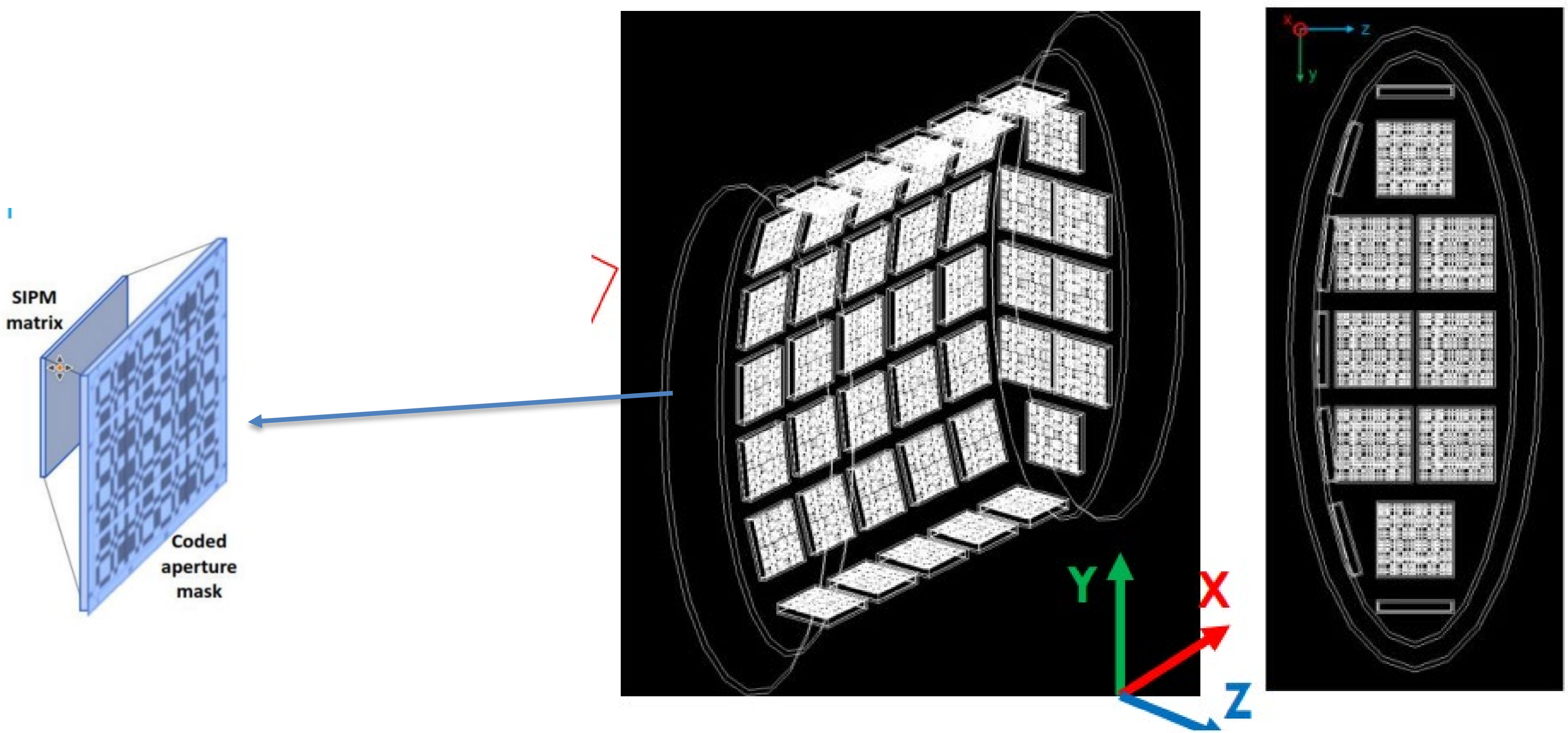

GRAIN: Analytic Approach

3D reconstruction:
front-to-front lenses and using theoretical P, P′ and F

$$X_s = -\frac{2cx'(x^2+y^2)}{f(x^2+y^2+xx'+yy')}$$

$$Y_s = -\frac{2cy'(x^2+y^2)}{f(x^2+y^2+xx'+yy')}$$

$$\mathbf{x} = (x, y), \qquad \mathbf{x}' = (x', y')$$

c distance of the center of the lens from the center of GRAIN

f lens-sensor distance

WARNING: the labels X_s and Y_s are meant as the transversal 3D coordinates to the projection direction

3D RECONSTRUCTION WITH CODED APERTURE MASKS

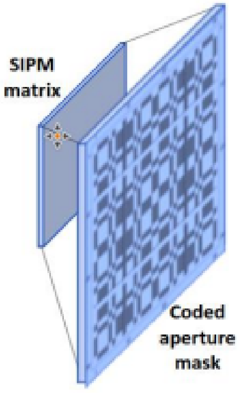

Coded aperture mask techniques were developed as the evolution of a single pinhole camera

Matrix of multiple pinholes to improve light collection and reduce exposure time

Image formed on sensor is the superimposition of multiple pinhole images.

Advantages:

Good light transmission (50%)

Good depth of field

Small required volume

Detailed description of Hadamard masks and deconvolution methods:
Eur. Phys. J. C 81 (11) 1011 (2021)

Readout system with SiPM matrixes coupled with coded aperture masks.

The custom **reconstruction algorithm** produces a **3D map of the deposited energy**:

- measured incident photons are propagated back into the LAr volume with an appropriate weight assigned to voxels.
- This weight represents the Bayesian probability of the voxel to be a source of the detected photons.
- A score in the segmented reconstruction volume is calculated by adding these weights.

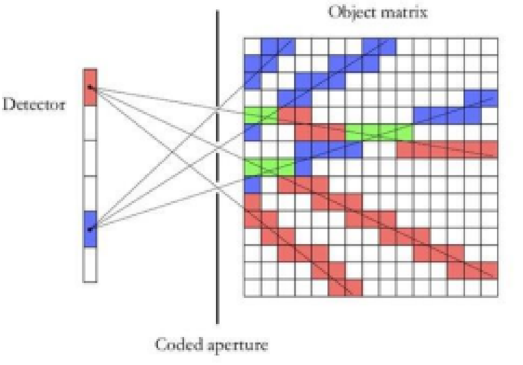

Electron ID

used for electron identification in ECAL in addition to the longitudinal profile. We combine the following 13 variables into a ANN: (a) E/p; (b) fraction of total energy deposited in the layer 1; (c) fraction of total energy deposited in the layer 2; (d) fraction of total energy deposited in the layer 3; (e) fraction of total energy deposited in the layer 4; (f) fraction of total energy deposited in the layer 5; (g) asymmetry (max-min)/(max-min) in the energy fractions among the 5 layers; (h) energy deposited in the first layer; (i) maximal energy in a cell within the first layer; (l) total number of cells with deposited energy; (m) number of cells in the first layer; (n) number of cells in the last layer; (o) ratio between the energy deposited in the central cell and the one in the surrounding cells in the last layer. Figure 147 shows the distribution of the NN output for electrons and pions and the corresponding sensitivity as a function of the NN cut. An electron efficiency of 90% corresponds to a pion efficiency of about 6.4%.

Proton/Pion

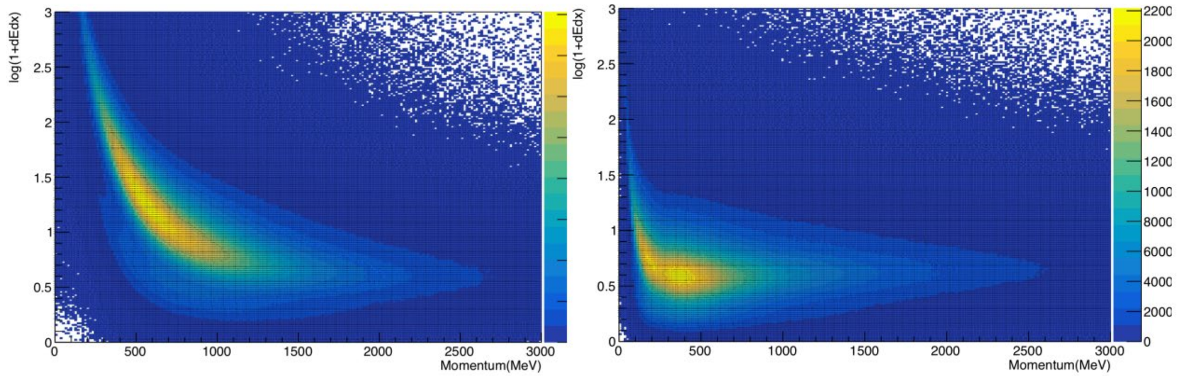

Figure 148: Distribution of $\log(1 + dE/dx)$ as a function of the momentum for protons (left plot) and pions (right plot) in STT. The energy deposition in the gas mixture Xe/CO_2 (or Ar/CO_2 for modules with graphite targets) of each straw crossed by the particle is used. Reconstruction effects are taken into account in the plots.

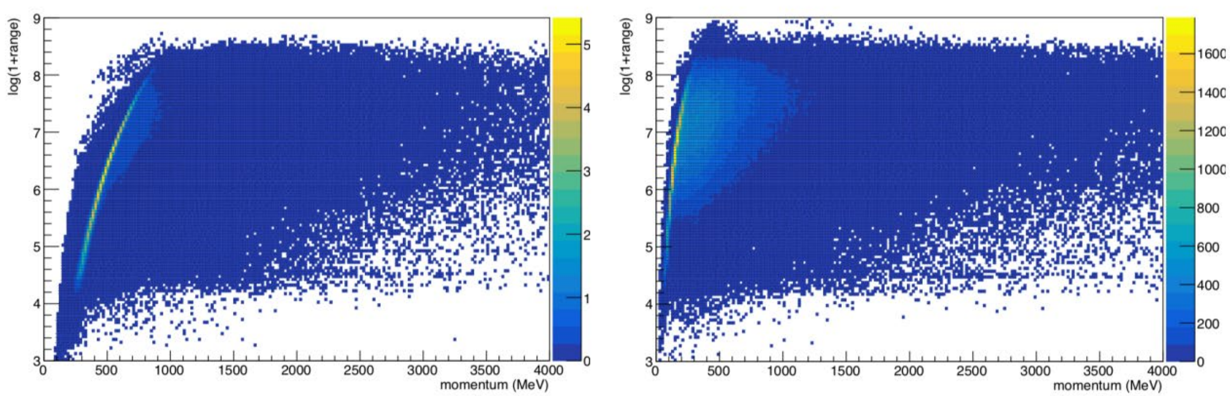

Figure 150: Distribution of $\log(1 + \text{range})$ as a function of the momentum protons (left plot) and pions (right plot) in STT. The range includes the various passive targets.

Proton ID with TOF and ECAL

$m = p/(\beta\gamma)$. We combined the following 7 variables into a ANN: (a) $\ln \lambda^{p/\pi}_{dE/dx}$ from dE/dx as described above; (b) total range; (c) momentum measured in STT; (d) β; (e) reconstructed mass m; (f) flag determining if the track reaches ECAL; (g) maximal number of cells in ECAL. Figure 152 shows the distributions of the corresponding NN output for protons and pions. With a 90% proton efficiency we obtain a pion efficiency of about 1.1%. The same NN can be used to veto protons in the kinematic tagging of the leading CC leptons described in Sec. 5.8.1. For this application we obtain a proton efficiency of 0.7% with a muon efficiency of 95% (Fig. 152).

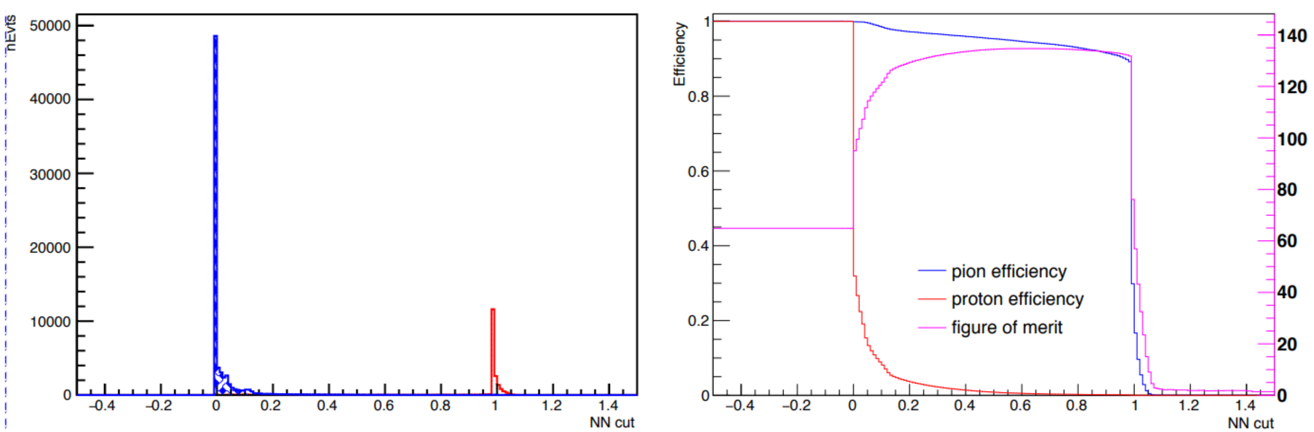

Figure 152: Distribution of the NN output for proton identification (left plot) and corresponding sensitivity as a function of the NN cut (right plot).

Muon ID (I)

surface, while a significant fraction of pions stop or interact within the first 4 ECAL layers. We subdivide the charged tracks in two categories: (i) tracks reaching the outermost layer 4; (ii) tracks stopping or interacting in layers 0-3. For both samples, we initially disregard the pions crossing all 5 ECAL layers without interacting and focus on the ones either stopping or interacting in ECAL. We start our identification algorithm from the first sample and select 10 discriminant variables: (a) maximal energy in a cell; (b) asymmetry in the cell energy (max-min)/(max+min); (c) total number of cells; (d) mean energy among the 5 layers; (e) RMS of energy among the 5 layers; (f) asymmetry in layer energy (max-min)/(max+min); (g) energy in outermost layer 4; (h) maximal energy in layers; (i) minimal energy in layers; (l) maximal number of cells in layers. Figure 154 shows the distributions of these variables for muon and pion tracks. We combine the 10 variables into an ANN and train it with all muon tracks (signal) and with the sub-sample of pions stopping or interacting in ECAL (background), as illustrated in Fig. 155. We select tracks with NN>0.28 as muon candidates, with an efficiency of 98% for actual muons and 7.5% for pions (Fig. 156).

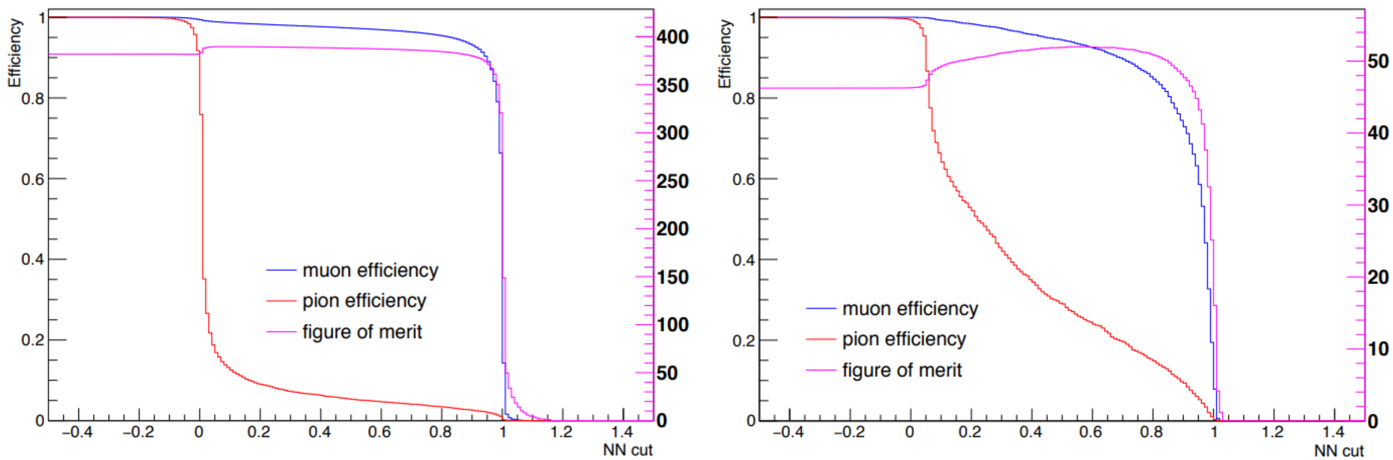

Figure 156: Muon and pion efficiencies and sensitivity $S/\sqrt{S+B}$ as a function of the NN cut for tracks with outermost energy in layer 4 (left plot) and the ones stopping or interacting in layers 0-3 (right plot).

Muon ID (II)

We apply a similar procedure for the second sample of tracks stopping or interacting within the first 4 ECAL layers. The following 8 discriminant variables are combined into an Artificial Neural Network (ANN): (a) maximal energy in a cell; (b) total number of cells; (c) mean energy among the layers; (d) asymmetry in layer energy (max-min)/(max+min); (e) maximal energy in layers; (f) minimal energy in layers; (g) range inside ECAL; (h) reconstructed momentum in STT. Figure 155 shows the ANN output. We select the cut NN>0.49 based on the global sensitivity $S/\sqrt{S+B}$ including the events from the other sample passing the cut in layer 4 (Fig. 156). The combined muon efficiency is 98% and the pion efficiency is 10.9%. So far we have ignored the pions crossing all the 5 ECAL layers – total thickness about one interaction length λ – without interacting. Figure 157 shows the distribution of the layer 4 NN output for this sample. The same NN cut above rejects about 43% of this pion sample, mainly due to the energy deposition in the ECAL layers. The total fraction of pions passing the NN selection in ECAL is 23.7%.

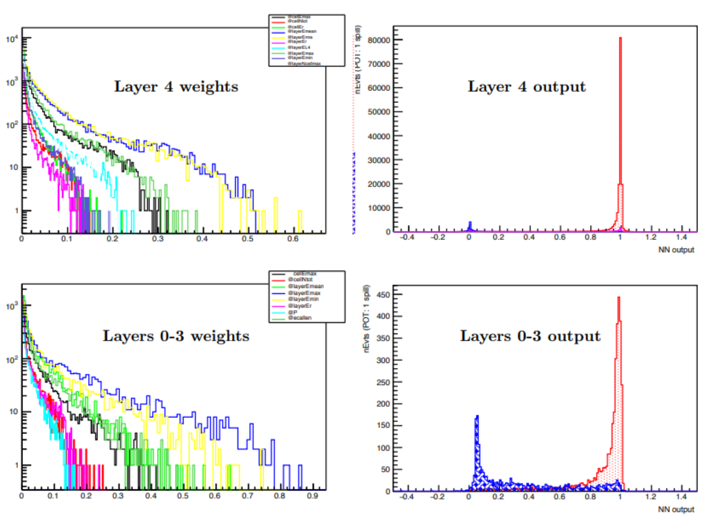

Figure 155: Weights of ANN variables (left plots) and ANN output (right plots) for muons and pions with outermost energy in layer 4 (top plots) and for the ones stopping or interacting in layers 0-3 (bottom plots).

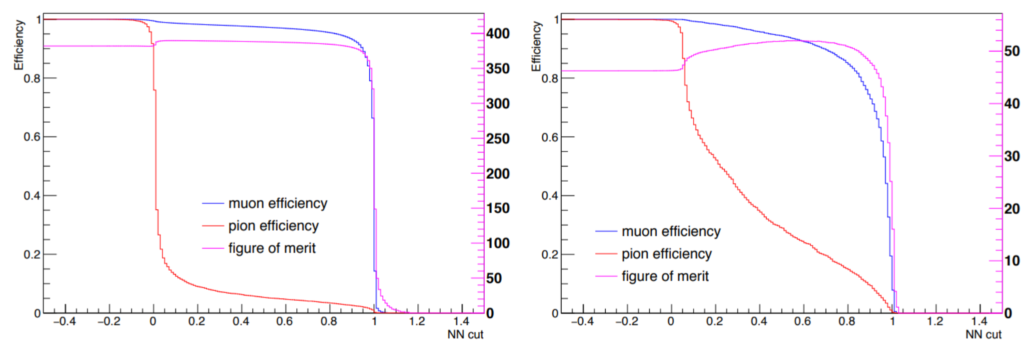

Figure 156: Muon and pion efficiencies and sensitivity $S/\sqrt{S+B}$ as a function of the NN cut for tracks with outermost energy in layer 4 (left plot) and the ones stopping or interacting in layers 0-3 (right plot).

Kinematical tagging of leading muon

system, since the total visible momentum vector is fixed (three constraints). We select the following four kinematic variables [23]:

- p_T^l: transverse momentum of the track candidate;
- $\theta_{\nu l}$: angle of the track candidate with respect to beam direction;
- y_{Bj}: ratio between the energy of the "hadron system" (visible energy minus track energy) and the total visible energy;
- R_{Q_T}: ratio between the transverse size of the of the "hadron system" $\langle Q_T^2 \rangle_H$ and that of the full event $\langle Q_T^2 \rangle$, where Q_T component of the track momentum perpendicular to the total visible momentum.

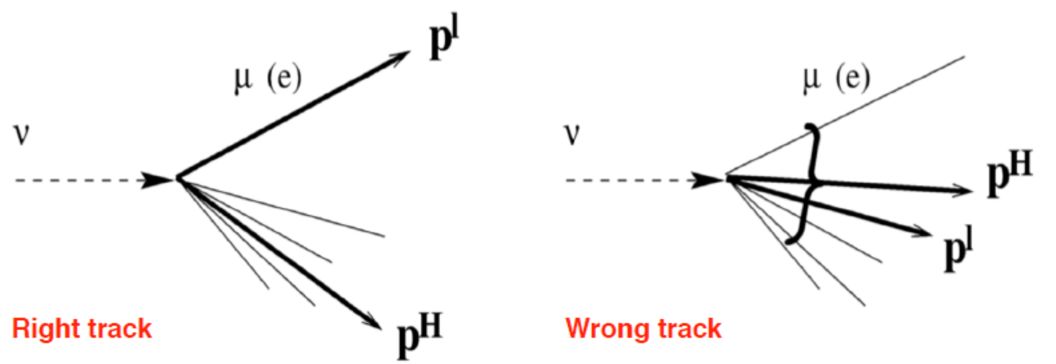

Figure 174: Illustration of the kinematic tagging in CC interactions. See text for details.

Kinematical tagging of leading muon

We combine the four kinematic variables into an ANN, which is trained with the true muon tracks (signal) and random hadron tracks from ν_μ ($\bar{\nu}_\mu$) CC interactions in the FHC (RHC) beam with a number of possible candidate tracks ≥ 2. In order to take into account the kinematic bias introduced by the magnet yoke we perform two separate trainings: (i) NN_1 using all candidate tracks; (ii) NN_2 using only candidate tracks not reaching the outer magnet yoke. Figure 177 shows the distributions of both the NN_1 and NN_2 outputs for true muons and random hadrons in ν_μ CC events.

The fist step of the muon tagging algorithm is the listing of all possible candidate tracks with the desired charge within the same event. We veto tracks which are interacting within the STT tracking volume and exclude them from the list of candidate tracks. Similarly, for the μ^+ tagging we apply a proton veto on all positive tracks not reaching the outer magnet yoke. This veto is based on a loose cut on the ANN for proton identification described in Sec. 5.4.2 and is required since protons typically have small momentum and are emitted at large angles, similarly to the muons not reaching the outer magnet yoke.

For events in which more than one candidate track is present, we then calculate the value of the tagging ANN for each candidate track. To this end, we use either the NN_1 training or the NN_2 training, depending on whether the track reaches the outer magnet yoke or not. In order to compare the numerical values of both trainings we multiply NN_2 by a scale factor $c = 15$, which was optimized by maximizing the overall muon tagging efficiency. We then rank all candidate tracks in descending order of the calculated value of the tagging NN. We select the most likely muon candidate as the single track with the highest rank in the list of all possible candidate tracks. Table 22 summarizes the resulting muon tagging efficiencies. Overall, we correctly select the true primary muon in 99.1% of the ν_μ CC events in the FHC beam and 99.3% of the $\bar{\nu}_\mu$ CC in the RHC beam. Figures 178 and 179 show the dependence of the tagging efficiency from the muon momentum.

Kinematical tagging of leading muon

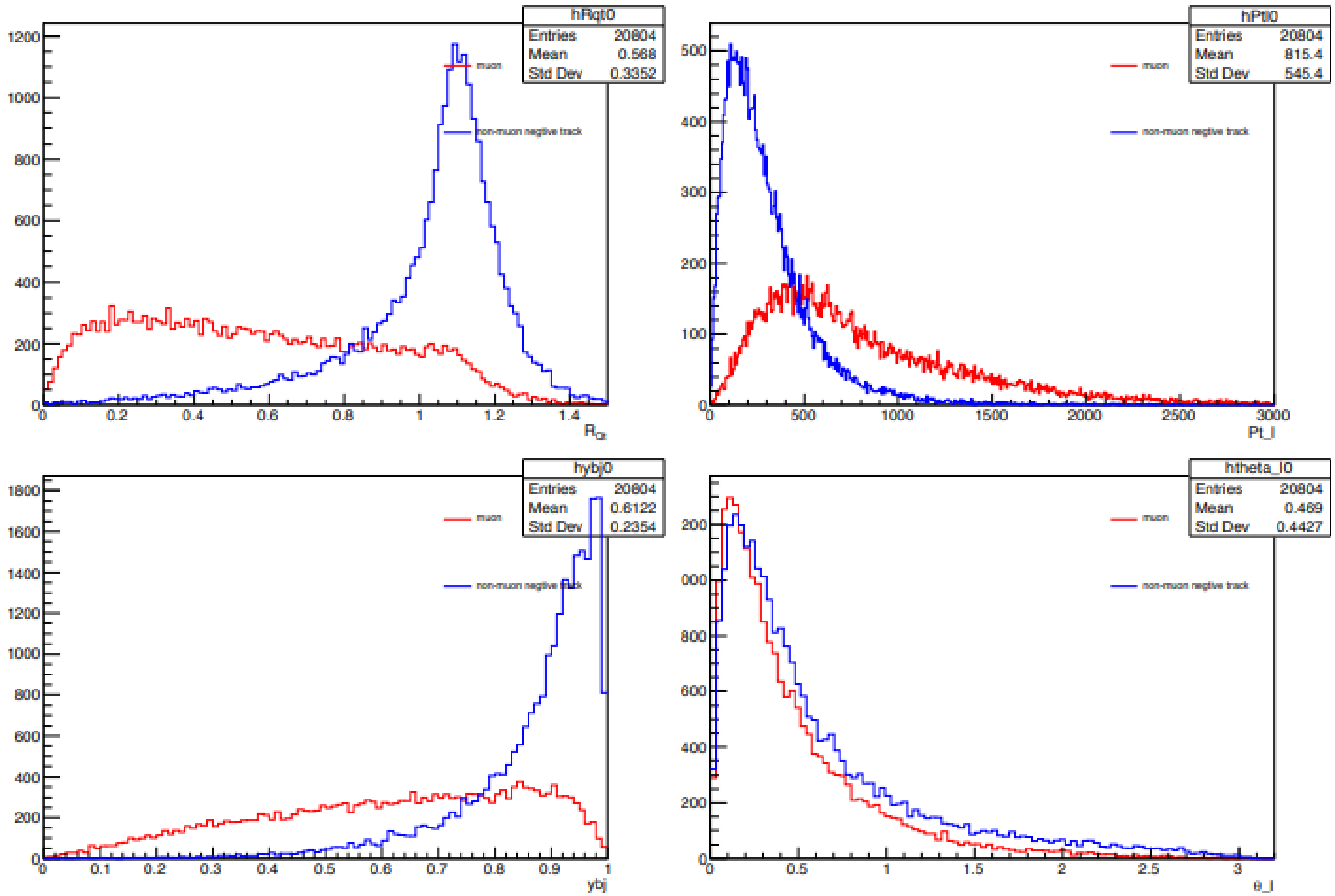

Figure 175: Kinematic tagging of μ^- in ν_μ CC from STT fiducial volume in the FHC beam: distribution of the kinematic variables used in NN_1 for all CC events with ≥ 2 negative tracks. See text for details.

Kinematical tagging of leading muon

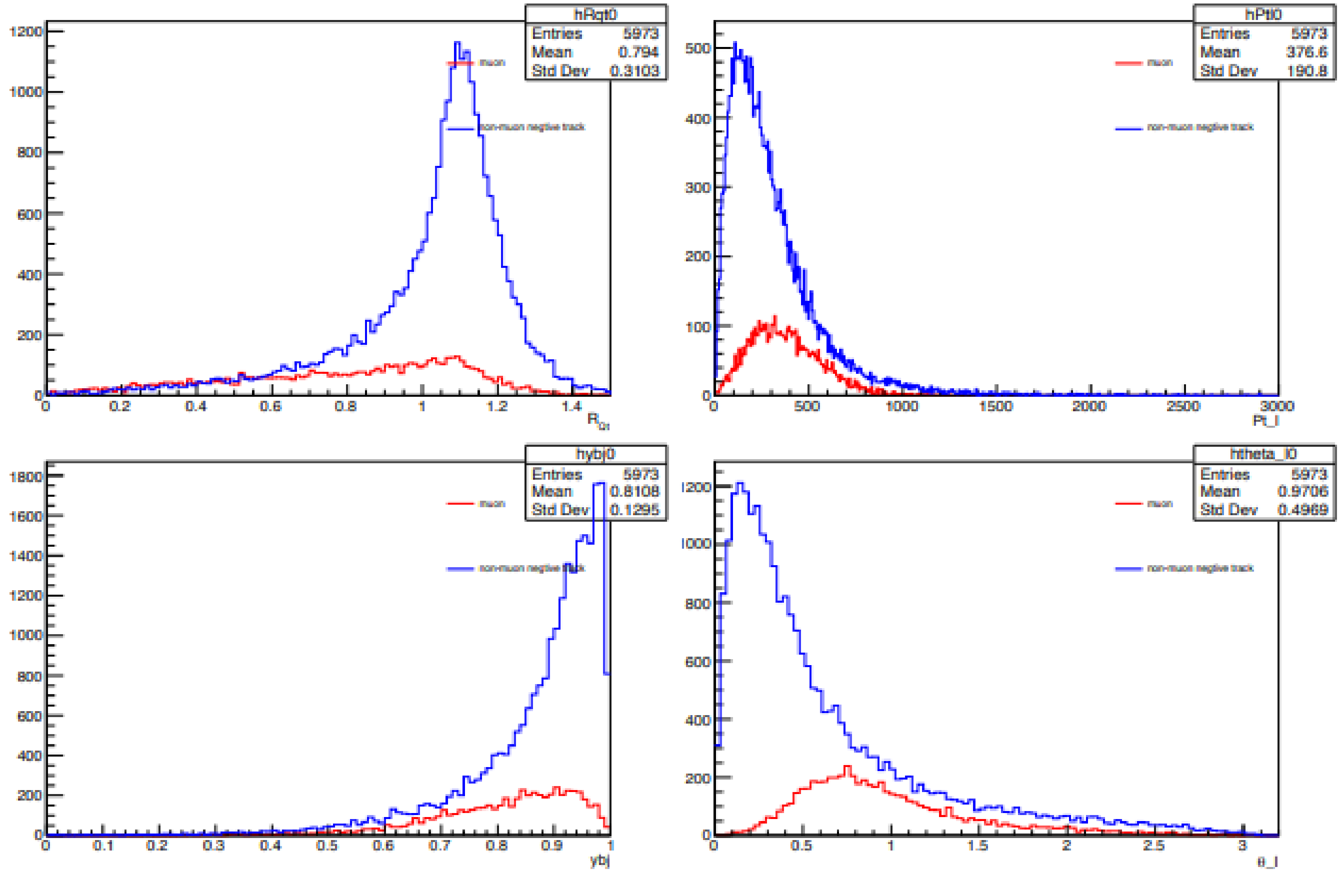

Figure 176: Kinematic tagging of μ^- in ν_μ CC from STT fiducial volume in the FHC beam: distribution of the kinematic variables used in NN_2 for all CC events with ≥ 2 negative tracks not reaching the outer yoke. See text for details.

Kinematical tagging of leading muon

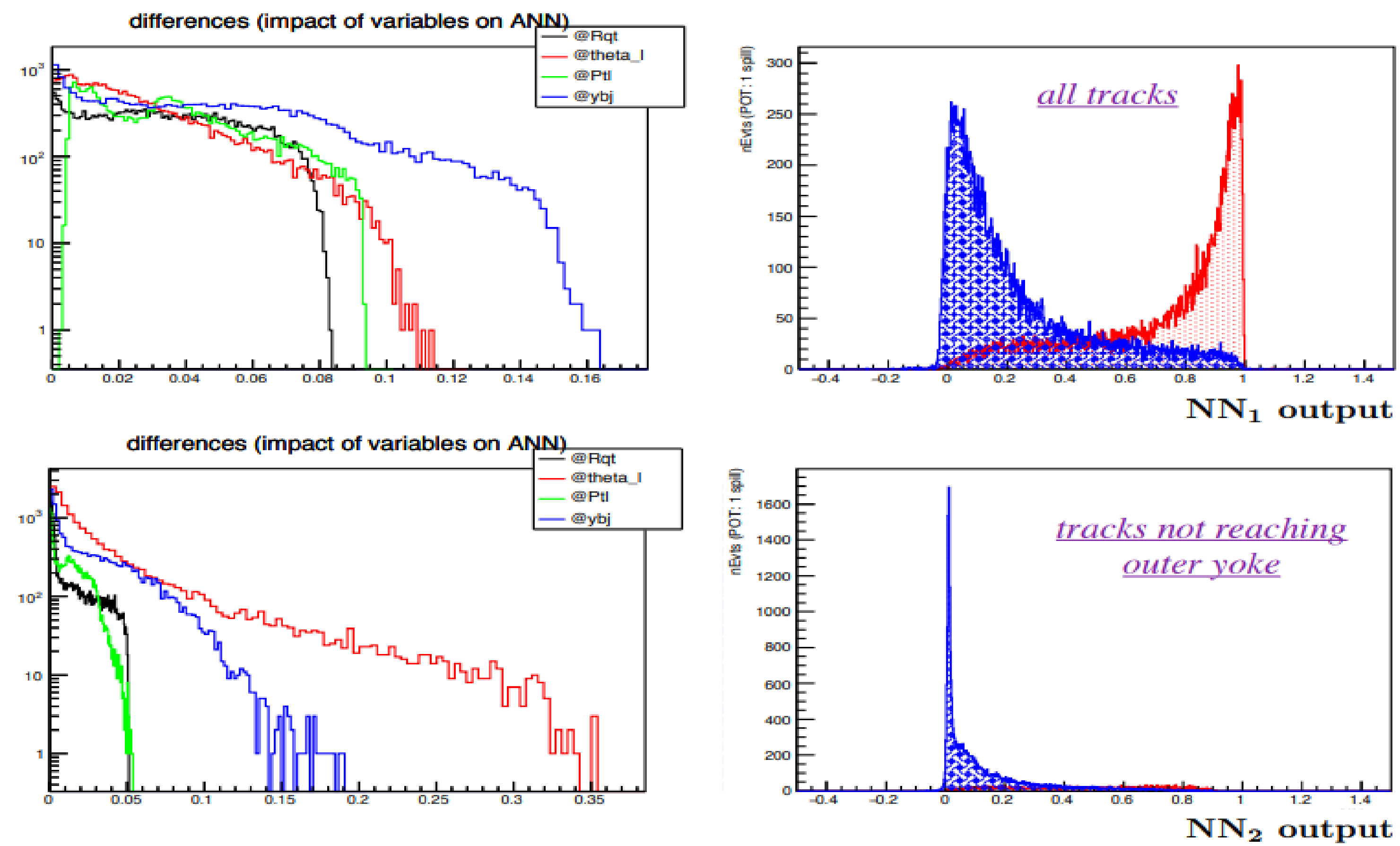

Figure 177: Weights of ANN variables (left plots) and ANN output (right plots) for μ^- (red) and random h^- hadrons from ν_μ CC interactions in FHC beam. Top plots: all tracks from CC events with ≥ 2 negatively charged candidates. Bottom plots: sub-sample of tracks not reaching the outer magnet yoke from CC events with ≥ 2 negatively charged candidates. See text for details.

Kinematical tagging of leading electron

The kinematic tagging of $e^{\pm}$ follows closely the algorithm described above for $\mu^{\pm}$. We list all possible track candidates with the correct charge within the same event, excluding tracks interacting within the STT volume. We apply a proton veto on positive tracks after re-training the corresponding NN for proton identification (Sec. 5.4.2) for the specific e/p separation, in order to take into account the different energy loss of electrons and pions/muons. For events with more than one candidate track, we then rank the $e^{\pm}$ candidates in decreasing order of the tagging NN_1. We use a single training since in the case of $e^{\pm}$ no kinematic bias is expected from the magnet yoke. To this end, we do not re-train the tagging ANN, but rather use the same training obtained from $\nu_\mu(\bar{\nu}_\mu)$ CC events. While slightly reducing the achievable tagging efficiency, this choice is primarily intended to reduce systematic uncertainties on the ν_e/ν_μ and $\bar{\nu}_e/\bar{\nu}_\mu$ ratios (Sec. 6.4). We select the most likely electron candidate as the single track with the highest rank. Table 22 summarizes the resulting electron tagging efficiencies. Overall, we correctly select the true primary electron in 98% of the ν_e CC events in the FHC beam and 98.6% of the $\bar{\nu}_e$ CC in the RHC beam.